Quantifying the diurnal variation of atmospheric NO₂ from observations of the Geostationary Environment Monitoring Spectrometer (GEMS)

David P. Edwards[1], Sara Martínez-Alonso[1], Duseong S. Jo[1,2], Ivan Ortega[1], Louisa K. Emmons[1], John J. Orlando[1], Helen M. Worden[1], Jhoon Kim[3], Hanlim Lee[4], Junsung Park[4,5], and Hyunkee Hong[6]

[1]Atmospheric Chemistry Observations & Modeling Laboratory, National Center for Atmospheric Research, Boulder, CO, USA.
[2]Seoul National University, Seoul, South Korea.
[3]Department of Atmospheric Science, Yonsei University, Seoul, South Korea.
[4]Division of Earth Environmental System Science, Pukyong National University, Busan, South Korea.
[5]Smithsonian Astrophysical Observatory, Cambridge, MA, USA.
[6]National Institute of Environmental Research, Seoul, South Korea

Correspondence to: David P. Edwards (edwards@ucar.edu)

Abstract. The Geostationary Environment Monitoring Spectrometer (GEMS) over Asia is the first geostationary Earth orbit instrument in the virtual constellation of sensors for atmospheric chemistry and composition air quality research and applications. For the first time, the hourly observations enable studies of diurnal variation of several important trace gas and aerosol pollutants including nitrogen dioxide (NO₂) which is the focus of this work. NO₂ is a regulated pollutant and an indicator of anthropogenic emissions in addition to being involved in tropospheric ozone chemistry and particulate matter formation. We present new quantitative measures of NO₂ tropospheric column diurnal variation which can be greater than 50% of the column amount especially in polluted environments. The NO₂ distribution is seen to change hourly and can be quite different from what would be seen by a once-a-day low Earth orbit satellite observation. We use GEMS data in combination with TROPOMI satellite and Pandora ground-based remote sensing measurements and MUSICAv0 3D chemical transport model analysis to examine the NO₂ diurnal variation in January and June 2023 over Northeast Asia and Seoul, South Korea, study regions to distinguish the different emissions, chemistry, and meteorological processes that drive the variation. Understanding the relative importance of these processes will be key to including pollutant diurnal variation in models aimed at determining true pollutant exposure levels for air quality studies. The work presented here also provides a path for investigating similar NO₂ diurnal cycles in the new TEMPO data over North America, and later over Europe with Sentinel-4.

1 Introduction

Predicting atmospheric air quality (AQ) requires understanding the processes that emit air pollutants, how these are transported in the atmosphere, the chemical and physical transformations that take place, and the potential impact on health and environment. Satellite observations provide valuable information on these processes, but until recently, measurements

from an individual platform were limited to twice daily at best when relying on observations from low Earth orbit (LEO). This is now changing with daylight hourly observations of atmospheric trace gases and aerosols from the new geostationary Earth orbit (GEO) satellite sensors. The South Korean GEO-KOMPSAT-2/GEMS (Geostationary Korea Multi-Purpose Satellite-2/Geostationary Environment Monitoring Spectrometer) instrument (Kim et al., 2020) has been operational over Asia since February 2020, NASA's EVI-1 TEMPO (Earth Venture Instrument-1 Tropospheric Emissions: Monitoring Pollution) (Zoogman et al., 2017), was launched in April 2023 to monitor North America, and Europe will be covered by ESA/EUMETSAT Sentinel-4 (Bazalguette Courrèges-Lacoste et al., 2013) in 2025. Common objectives for these missions will provide column products for ozone (O_3), nitrogen dioxide (NO_2), sulfur dioxide (SO_2), formaldehyde (HCHO), and aerosol optical depth, among others, several times per day at 5–10 km/pixel spatial scales. Together with LEO sensors such as JPSS/CrIS (Joint Polar Satellite System/Cross-track Infrared Sounder) (Han et al., 2013), MetOp/IASI (Infrared Atmospheric Sounding Interferometer) (Clerbaux et al., 2009), and Sentinel 5-P/TROPOMI (TROPOspheric Monitoring Instrument) (Veefkind et al., 2012), the new GEO missions will form an atmospheric composition satellite virtual constellation with nearly continuous Northern Hemisphere coverage and unprecedented capability to meet the needs of AQ research and applications (CEOS, 2019).

The measurement hourly time resolution is the novel perspective provided by the new GEO platforms that enables: (1) investigations of the diurnal processes determining atmospheric composition; (2) improvements in retrieval sensitivity gained with possible longer measurement acquisition dwell times; (3) high observation data density; and (4) the increased probability of obtaining at least some daily cloud-free observations at any given location (e.g., Fishman et al, 2012; Zoogman et al., 2017; Kim et al., 2020). An important role for the GEO sensors will be in detailing how the new hourly information improves our understanding of diurnal changes that take place with pollutant emissions and subsequent chemistry and transport and how this leads to diurnal changes in AQ, In urban and polluted regions where these diurnal changes are large, this will likely lead to revised estimates for emissions, population exposure, and associated health and environmental risks compared to those previously based on LEO measurements. This work investigates the processes that drive the diurnal variation of NO_2 over Northeast Asia, and particularly over Seoul, South Korea, using GEMS data in combination with other satellite and ground-based remote sensing measurements and 3D atmospheric chemical transport model (CTM) analysis

Of the trace gas products that are routinely retrieved from satellite sensor shortwave spectral measurements, NO_2 is one of the most reliable due to the relatively strong signal. It plays a central role in atmospheric chemistry and tropospheric O_3 and aerosol formation and is photochemically linked with nitrogen oxide (NO) as reactive nitrogen ($NO_x \equiv NO+NO_2$) (Brasseur et al., 1999). NO_x emissions occur primarily as NO and have anthropogenic sources associated with high temperature combustion processes in the power, industry, and transport sectors (e.g., Goldberg et al., 2021; de Foy et al., 2022). Natural sources include lightning, biomass burning, and soil emissions amongst others (e.g., Griffin et al., 2021; Huber et al., 2020). The NO_2 minutes-to-hours daytime lifetime in the planetary boundary layer (PBL) also means that it does not become evenly

65 mixed in the atmosphere, and polluted regions, especially urban areas, often show satellite-derived NO₂ column enhancements of many times the background level. These products are therefore particularly useful for understanding NO_x and other emissions and their subsequent chemical and physical transformations along with attributing pollution trends over time due to emission regulations and other factors such as the COVID pandemic lockdowns and economic downturns (e.g., Duncan et al., 2013; Levelt et al., 2022; deRuyter de Wildt et al., 2012). This has resulted in a wealth of peer-reviewed

70 literature based on LEO satellite observations detailing pollutant research and AQ applications and management (e.g., Curier et al., 2014; Duncan et al., 2016; Liu et al, 2017). The partitioning of NO_x between NO and NO₂ is in photochemical steady state that establishes on a timescale of minutes during daylight hours. Details are given in Brasseur et al. (1999) and the NO_x ratio can be represented as:

$$[\text{NO}]/[\text{NO}_2] = j_{NO2}/(k_{O3}[O_3] + k_{HO2}[HO_2] + k_{RO2}[RO_2]) \tag{1}$$

75 where the square bracket denotes concentration (molec.cm⁻³), k is a bimolecular rate coefficient (cm³.molec⁻¹.sec⁻¹), and j is the photolysis rate (sec⁻¹). HO_2 is the hydroperoxy radical and RO_2 represents all organic peroxy radicals. The main loss of NO_x is through oxidation to the nitrogen reservoirs nitric acid (HNO_3) and peroxyacetyl nitrate (PAN). The chemical diurnal cycle is discussed further in Section 5.3 based on the GEMS NO₂ data and modeling.

Following this Introduction, Section 2 describes the remote sensing measurements and the model tools that are used in this

80 work. Section 3 presents the NO₂ diurnal variation observed by GEMS at different spatial scales for our January and June 2023 study months, and this is compared with ground-based remote sensing measurements over Seoul in Section 4. Model analysis and discussion in Section 5 considers the various processes (emissions, chemistry, and meteorology) that drive the NO₂ diurnal variation. Conclusions are presented in Section 6.

2 Observations and modeling tools

85 ### 2.1 GEMS

South Korea's GEMS is the first satellite instrument in the GEO constellation and is monitoring AQ over Asia. GEMS was launched in February 2020 by Arianespace from the French Guiana Space Center. Like the TEMPO instrument, GEMS was built by Ball Aerospace & Technologies Corp. GEMS retrievals of O_3, NO₂, SO_2, HCHO, glyoxal (CHOCHO), and aerosols are derived from ultraviolet-visible (UV-vis) measurements (Kim et al., 2020), and the cloud fraction necessary for data

90 filtering is also available for each observation (Choi et al., 2020; Kim et al., 2024). Each day, the field of regard (FOR) shifts westward with the Sun providing measurements over India at the end of the day at the expense of losing coverage over Japan when the solar zenith angles become too large. Total column (TotC), stratospheric column (StrC), and for some products, tropospheric column (TrC) values are retrieved in up to 10 hourly observations during daytime according to the season with spatial resolution at Seoul near 7 x 7.7 km² for gases and cloud, 3.5 x 7.7 km² for aerosol and surface reflectivity.

95 The main retrieval challenges for NO$_2$ (e.g., Palmer et al., 2001; Buscela et al., 2013; Lorente et al., 2017; Geddes et al., 2018; Zara et al., 2018; van Geffen et al., 2020, Park, 2022b) are the conversion of the observed NO$_2$ slant column density to an inferred vertical column density using an air mass factor (AMF), and the separation of the StrC and TrC. These steps can both lead to significant uncertainties and biases as is well-documented in studies comparing the varying results from different NO$_2$ retrieval algorithms using the same OMI (Ozone Monitoring Instrument, Levelt et al., 2018) satellite

100 measurements (Zara et al., 2018). The AMF is primarily a geometric conversion based on the observation angles, but this must also consider other factors including cloud and aerosol information, terrain reflectivity, and vertical gas profile (Lorente et al., 2017). A CTM is used in this AMF calculation and also in the separation of the StrC and TrC (Lee et al., 2020; Geddes et al., 2018). The NO$_2$ a priori profiles in this GEMS data version are provided by the GEOS-Chem model (Bey et al., 2001). Although beyond the scope of this paper, retrieval sensitivity studies and product validation for the new GEO composition

105 measurements will be important to minimize any aliasing of diurnal variation in the retrieval input parameters onto the diurnal variation of the retrieved products themselves (e.g. Yang et al., 2023a; Kim et al., 2023; Szykman and Liu, 2023). This includes, for example, parameters that impact the AMF, a priori that changes by location and time, angular dependences of surface and cloud reflectivities, vertical profiles of trace gases and aerosols, meteorology, and PBL evolution.

This work uses the publicly available Version 2 (V2.0) NO$_2$ Level 2 data obtainable from the Korean National Institute of

110 Environmental Research (NIER) (NIER, 2024). An example coverage is shown in Fig. 1. The data quality flags used are those recommended by the algorithm development team (Lee et al., 2022). These are: FinalAlgorithmFlags $\leq$1; CloudFraction <0.3; and SolarZenithAngle and ViewingZenithAngle $\leq$70°. The nominal GEMS pre-launch accuracy for the NO$_2$ TrC is 1×10^{15} (molec.cm^{-2}) (Kim et al., 2020). The Level 2 data contain an error term for the NO$_2$ spectral fit, but this does not account for the AMF calculation error and the conversion to vertical column. Analysis for TROPOMI (van Geffen

115 et al., 2022) identified the latter as the main source of product error (around $\pm$25 % over polluted regions). Comparison of the GEMS L2 NO$_2$ with other measurements is further discussed in Section 4. Updates and enhancements to the GEMS retrieval algorithms are ongoing and will result in new data versions being released periodically.
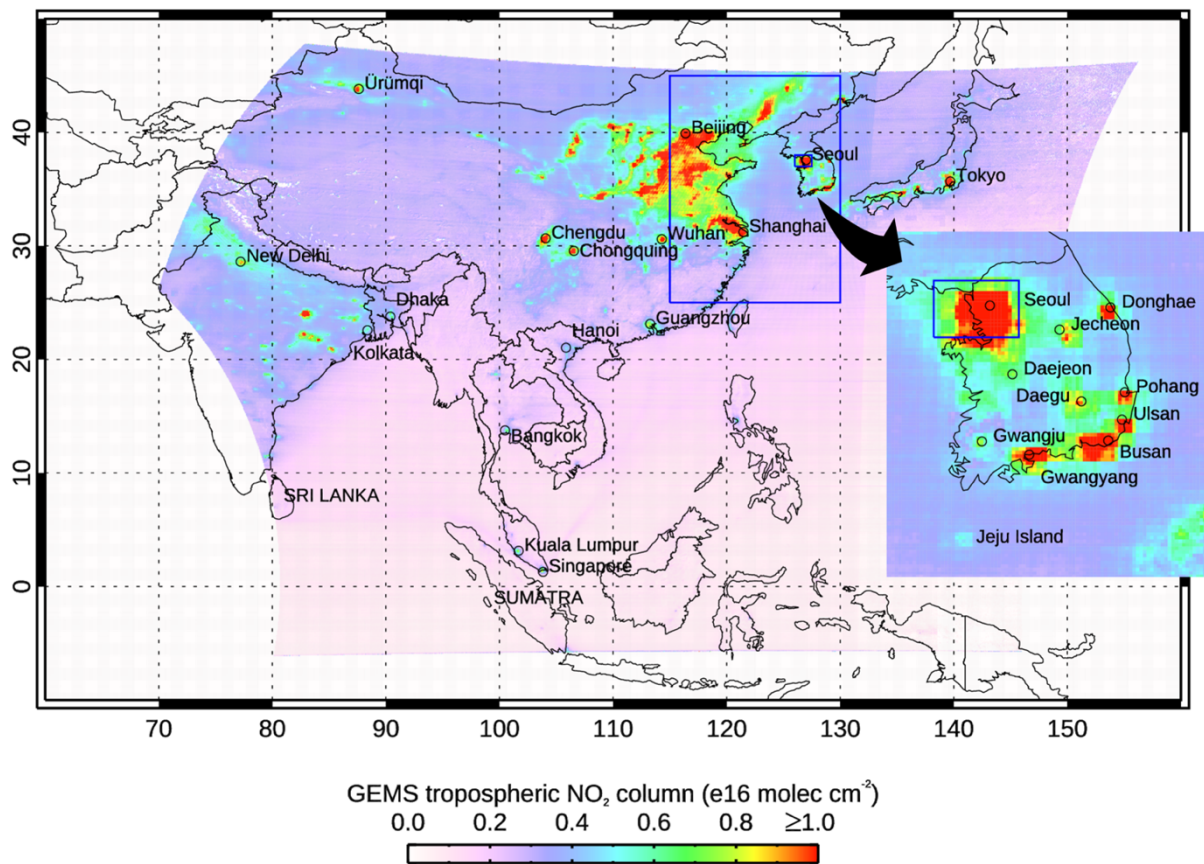
Figure 1: Averaged GEMS NO$_2$ TrC for June 2023 showing the full extent of the instrument FOR. Blue boxes indicate the Northeast Asia and Seoul study regions; see text for details. The color discontinuity near 130° E is due to the lower number (4) of daytime hourly observations towards the East compared to the 10 daytime hourly observations in the center of the domain that result from the FOR shifting westward with the Sun during the day.

2.2 TROPOMI

TROPOMI is a push-broom imaging spectrometer on ESA's Sentinel 5-Precursor satellite in a sun-synchronous orbit with a 13:30 local standard time Equator crossing (Veefkind et al., 2012). TROPOMI achieves close-to-global daily coverage at resolutions down to 3.5 x 5.5 km^2, depending on species. NO$_2$, HCHO, carbon monoxide (CO), SO$_2$, O$_3$, methane (CH$_4$), aerosol, and cloud are retrieved from UV-vis and reflected shortwave infrared measurements. We use the TROPOMI operational Level 2 data from Collection 3 that are publicly available through the NASA Earthdata portal (Earthdata, 2024).

2.3 NASA/ESA PANDONIA Global Network (PGN)

130   To capture time resolved measurements of highly variable species such as NO_2 in a coordinated manner, NASA initiated a large-scale global monitoring network of (quasi-) autonomous stations with the ground-based remote sensing spectrometer system called Pandora (Herman et al., 2009; Spinei et al., 2018). ESA joined this project in 2018 to form the Pandonia Global Network (PGN), which ensures systematic processing and dissemination of the data in support of AQ monitoring and satellite validation. Pandora instruments measure in the UV-vis and retrieve column amounts of several air pollutants

135   including NO_2, HCHO, and O_3. Data are publicly available (PGN, 2023).

2.4 Atmospheric chemistry model framework

The Multi-Scale Infrastructure for Chemistry and Aerosols (MUSICA) is a new community CTM for simulations of large-scale atmospheric phenomena in a global modeling framework, while still resolving chemistry at emission and exposure relevant scales (Pfister et al., 2020). In this work, we use MUSICA Version 0 (MUSICAv0) which is a configuration of the

140   Community Atmospheric Model with chemistry (CAM-chem) (Tilmes et al., 2019; Emmons et al., 2020) using a spectral element (SE) grid with regional refinement (RR) (CAM-chem-SE-RR), e.g., (Lauritzen et al., 2018; Schwantes et al., 2022). MUSICAv0 is run with a horizontal resolution of $0.0625°$ (~7 km) over refined regions selected to cover the Korean and wider Asian domain (Jo et al., 2023) and allows near matching of the GEMS pixel resolution of 7×7.7 km^2 over Seoul (see Fig. S1 of Jo et al., 2023). Chemical processes are all simulated in CAM-chem, which includes chemistry feedback on the

145   meteorology (e.g., aerosol-cloud interactions). To reproduce the dynamics for the January and June 2023 months analyzed, the capability of CAM-chem to nudge the model meteorology to GEOS5 $0.25°$ resolution reanalysis outside of the refined domain is used following Jo et al. (2023). Inside of the refined domain, the wind fields are calculated by the model. We stress that this work does not aim for exact model simulations of the GEMS data. Rather the model is used to investigate the processes driving the observed NO_2 diurnal variation.

150   Date-specific anthropogenic, biomass burning, and biogenic emissions are used in the simulations. The Copernicus Atmospheric Monitoring System version 5.1 (CAMS-GLOB-ANTv5.1) global emission inventory (Soulié et al., 2023) serves as the base anthropogenic emissions inventory along with the NIER/KU-CREATE inventory for East Asia and the Korean peninsula that was produced for the Korea-United States Air Quality Study (KORUS-AQ) field campaign in May-June 2016 (Jang et al., 2019; Park et al., 2021; Crawford et al., 2021). Global biomass burning emissions are provided as $0.1°$

155   resolution daily averages by the Quick-Fire Emissions Dataset (QFED) version 2.5_r1 (Koster et al., 2015) and Fire INventory from NCAR (FINN) v1.5 (Wiedinmyer et al., 2011). Biogenic emissions are simulated using the MEGAN v2.1 algorithm (Guenther et al., 2012), which is incorporated in the Community Land Model (CLM) (Lawrence et al., 2019) and calculated at each model timestep using the model meteorology. Global inventories of anthropogenic emissions are usually provided as monthly means that are temporally interpolated to a particular day by the model. However, the diurnal variation

160   of emissions also becomes important at the high spatial resolution of the MUSICAv0 refined grid. Diurnal emissions profiles have been derived for different sectors by country in the Emissions Database for Global Atmospheric Research (EDGAR)

and can be applied to other inventories (Crippa et al., 2020; Jo et al., 2023).

For our simulations over Seoul presented in Section 5.1, we consider the diurnal variation of emissions using profiles based on area/point and mobile sectors developed for KORUS-AQ and described in application to modeling over Seoul by Jo et al. (2023). This is shown in Fig. 2 and predicts a pronounced increase in emissions with daytime activity and rush-hour peaks in the mobile emissions. As is discussed in Section 5.1, the assumed model emissions diurnal profile can make a significant difference to the calculated TrC. We here include Fig. 2 showing the shape of the diurnal emissions to help in the interpretation of the results of Section 5.1 (particularly Fig. 10).
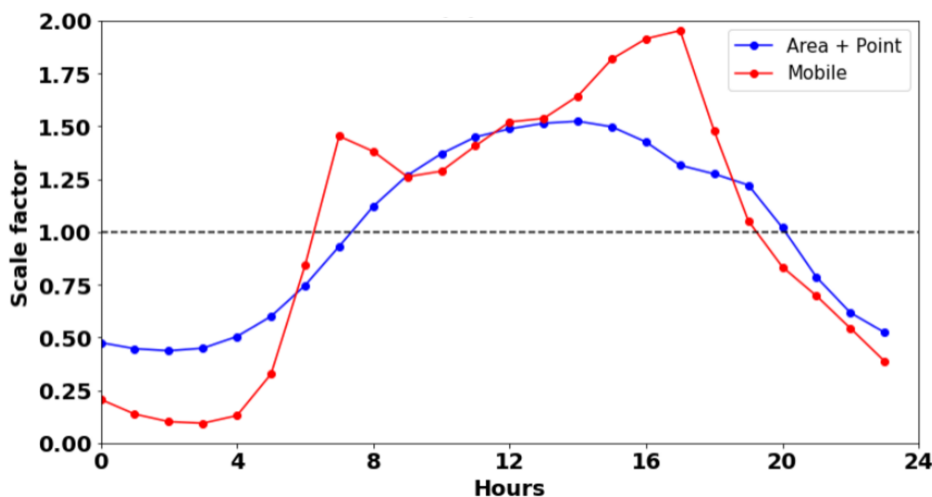
Figure 2: KORUS-AQ diurnal emissions profiles for the Area+Point and Mobile sectors.

Quantitative comparison of satellite retrievals and model simulations requires consideration of the measurement sensitivity to the target quantity and the retrieval a priori assumptions. These can be accounted for by applying the retrieval averaging kernels that formally relate the retrieved quantity to the true atmosphere (Rodgers, 2000). For retrieval/model comparisons of trace gas TrC from GEMS-like sensors, the averaging kernels allow a retrieval-consistent TrC to be derived from the model trace gas profile, or alternatively, a model-consistent TrC to be calculated from the retrieval by substituting the retrieval a priori trace gas profile used in the AMF calculation by the model profile (e.g., Boersma et al., 2016). However, there are known issues with the GEMS V2 processing of the NO_2 averaging kernels and the values reported in the operational data files, such that these should not be used as per guidance from NIER. The intention of the GEMS project is to remedy this issue with the next GEMS Version 3 release. Any independent or alternative reprocessing of the GEMS data to calculate averaging kernels is beyond the scope of this work. As a result, we are unable to perform quantitative model comparisons of the GEMS V2 products at this time and the comparisons with MUSICAv0 presented in Section 5 should be considered mainly qualitative for now.

3 GEMS observed NO₂ diurnal variation

3.1 Hourly measurements

An example of the ten GEMS daytime retrievals of NO₂ TrC over Northeast Asia (115°–130° E, 25°–45° N) for the
relatively clear day of 15 June 2023 is shown in Fig. 3. High NO₂ is seen over the Beijing region and the industrial areas of
the North China Plain. Pollution is also high over Shanghai and the Yangtze Delta with another hotspot over Seoul in South
Korea. The most striking first impression of this GEO perspective on atmospheric composition is how large the temporal
variation of the pollution is in magnitude as well as how much the spatial distribution shifts hour-by-hour. In certain
locations, changing cloud fields do not permit for all ten possible retrievals to pass the data filters. However, the hourly
observations do provide at least some measurements, thus demonstrating an advantage of the GEO perspective. During the
winter months when the sun is low in the sky, there are fewer GEMS hourly retrievals. The example is shown in Fig. 4 for
30 January 2023 NO₂ TrC over Northeast Asia. Compared to Fig. 3 (which uses the same color scale), the NO₂ burden is
considerably higher because of reduced NOₓ photochemical loss and NO₂ TrC build-up during the day. This results in less
diurnal variation compared to the summer months and is discussed in Section 5. The East-West data stripes evident in Fig.3
exist in this data version across the domain, similar to the spurious across-track variability issue for OMI. Zhang et al. (2023)
comment that this is likely associated with the specific scan modes of GEMS as well as periodically occurring bad pixels.
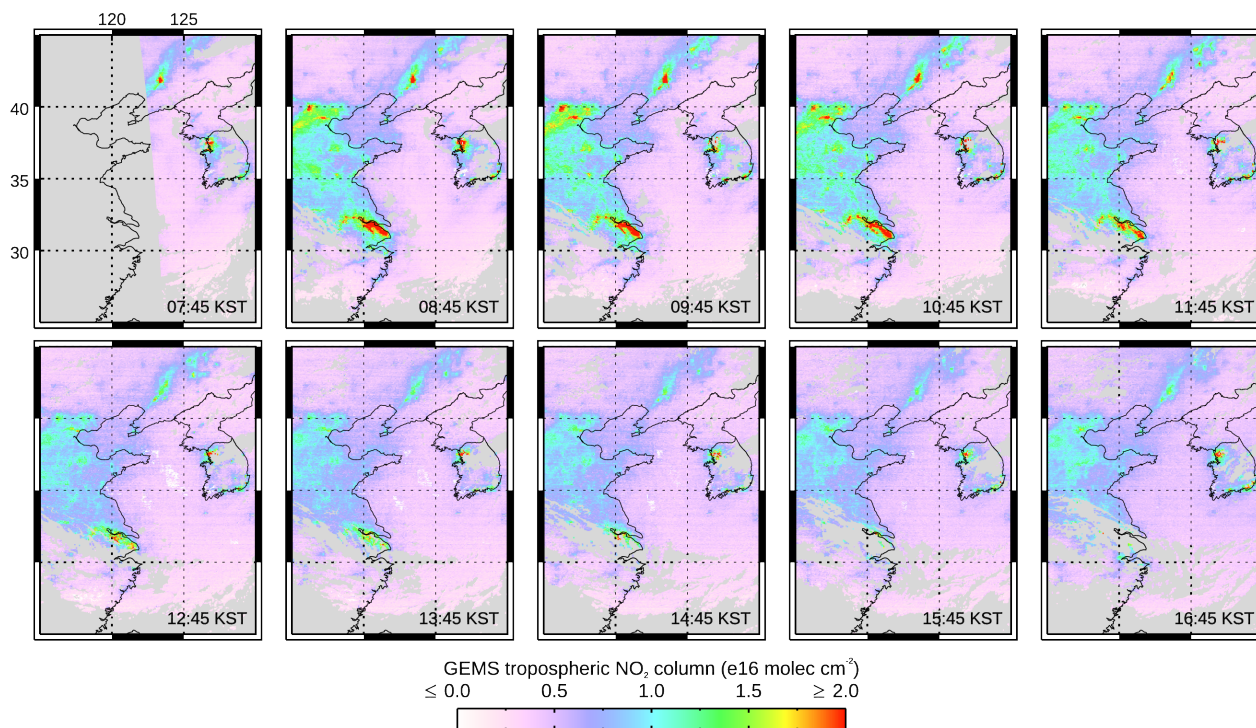
200 **Figure 3:** Northeast Asia NO$_2$ TrC hourly values, 15 June 2023. Observation times are quoted at Korean Standard Time (KST), i.e., Coordinated Universal Time (UTC) plus 9 hours. Gray indicates no data were taken during night-time or missing data due to clouds.
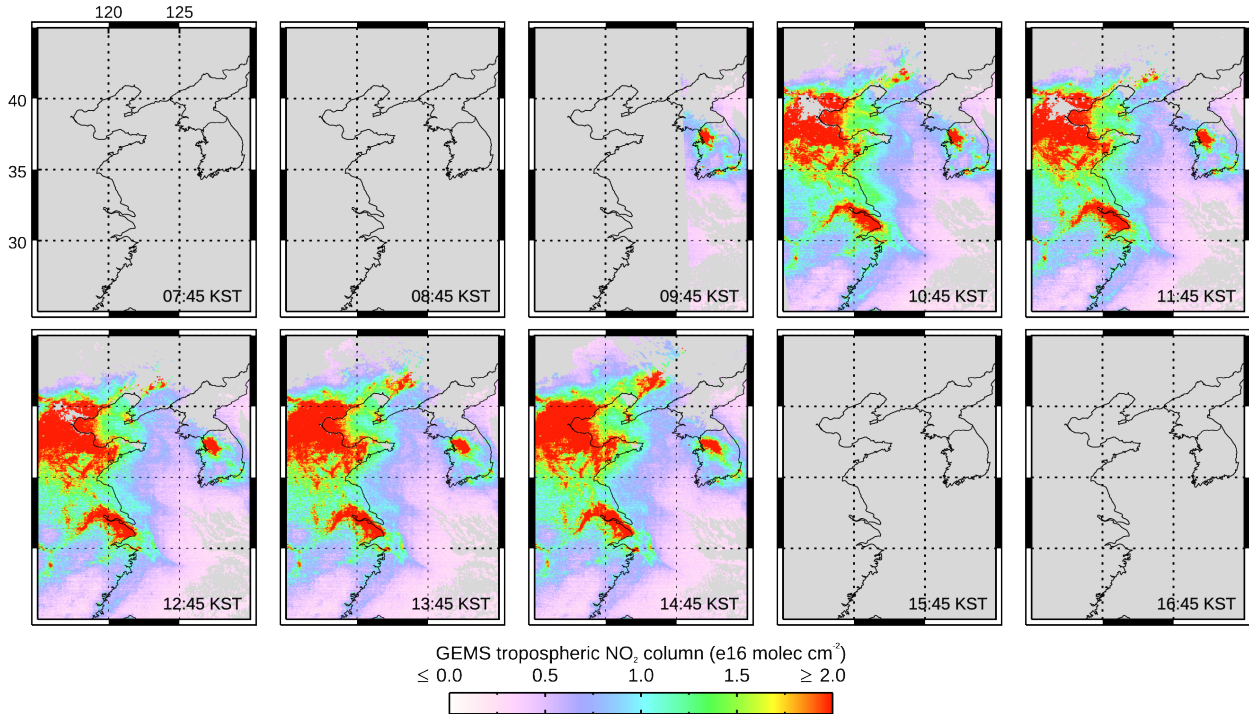
Figure 4: Same as Fig. 3 but now for 30 January 2023 NO$_2$ TrC.

205 **3.2 Quantifying GEMS NO$_2$ diurnal variation**

We have developed quantitative measures of the magnitude of the GEMS NO$_2$ TrC daily absolute and relative variation. The first of these, *ADV* (absolute daily variation), represents the absolute change in NO$_2$ TrC for a given day and pixel location as sampled by multiple hourly GEMS observations:

$$ADV_{i,j} = \sum_{k=1}^{n-1} \left| \left(TrC_{i,j,k} - TrC_{i,j,k+1} \right) \right| \tag{2}$$

210 where the pixel longitude and latitude are indexed by *i* and *j*, respectively, and *k* is the index of the GEMS hourly observation from 1 to *n*, for *n* being the number of useful cloud-free observation during the day. *ADV* is calculated for adjacent hourly observations, regardless of gaps due to missing data (gaps along a slope would have no effect on the resulting *ADV* value,

 Fig. 5 shows the monthly average of *ADV* for June 2023. Because this quantity depends on the number of useful cloud-free retrievals during the day, it is only calculated
215 for days and locations where there are at least 5 hourly observations, and it thus represents a lower bound on the total TrC change. No values are mapped east of ~130º E because there are too few daytime hourly observations at these locations. High variation usually coincides with locations of high TrC, such as industrial regions and cities, and illustrates the importance that time-resolved observations will have for characterizing changing NO_x emissions and population pollution exposure. Chinese and Korean cities are particularly noticeable as are Indian power facilities. Ship tracks between Hong
220 Kong and Singapore as well as between Sri Lanka and the northern tip of Sumatra were previously identified in GOME, SCIAMACHY, OMI, and TROPOMI NO_2 data, among others (Beirle et al., 2004; Richter et al., 2004; Franke et al., 2009; Georgoulias et al., 2020). The ship tracks in Fig. 5 show diurnal variation most likely because of horizontal dispersion with the increasing afternoon marine boundary layer. Averaging data temporally in this way at a given location reduces the contribution of transient emission or transport events that can produce significant day-to-day variation in the NO_2 TrC. The
225 averaged diurnal variation is then primarily dependent on emission and chemistry processes that occur on most days and thus indicates polluted urban regions in particular.
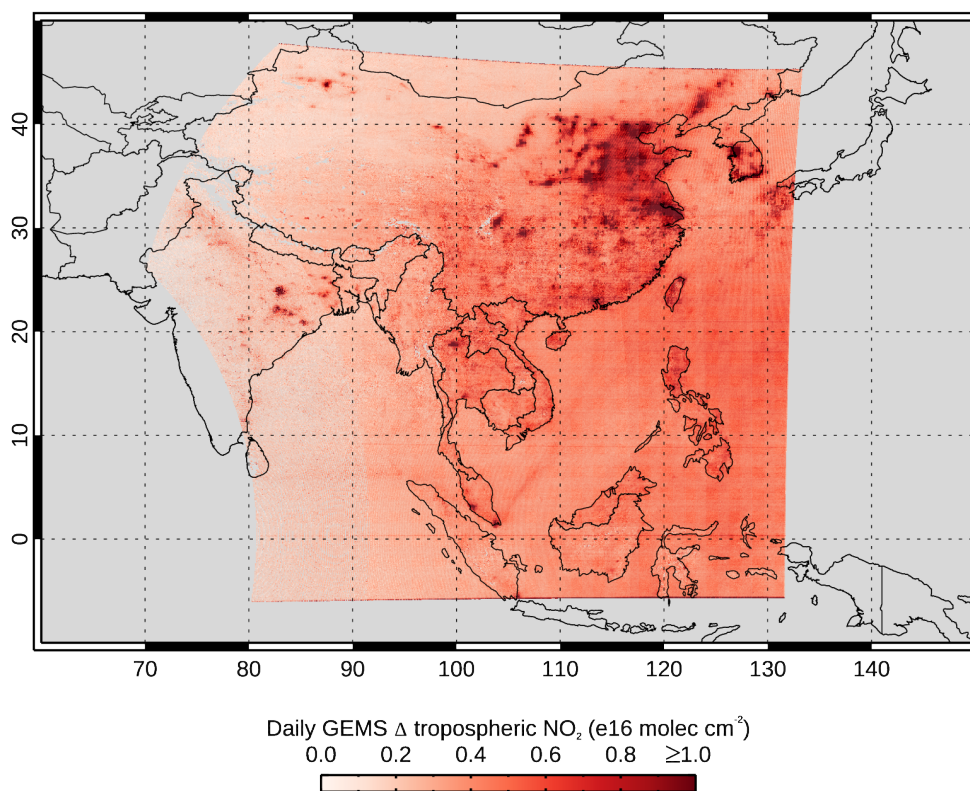
Figure 5: Monthly average of the absolute daily variation (*ADV*) in the GEMS NO_2 TrC for June 2023. The region east of

~130° E is not mapped because only data points with 5 or more observations per day were included in this analysis.

230 A second measure we consider relates the magnitude of the GEMS NO$_2$ TrC relative daily variation (*RDV*) over multiple hourly observations with respect to the value of the single observation that would be obtained from a LEO instrument such as TROPOMI. For a particular day and pixel location, the absolute deviation of the day's hourly observed NO$_2$ TrC relative to the observation at *t*=13:45 local time (closest to the TROPOMI overpass time) is calculated and normalized by the *t*=13:45 value:

235 $$RDV_{i,j} = \frac{1}{TrC_{i,j,t}} \sqrt{\frac{\sum_{k=1}^{n}\left(TrC_{i,j,k} - TrC_{i,j,t}\right)^2}{n}} \tag{3}$$

where *t* is the reference time (13:45 local standard time) and *n* is the number of observations at pixel location *i, j* excluding that acquired at the reference time. The daily *RDV* can then be averaged over the month as shown for June 2023 in Fig. 6. The monthly averaged *RDV* is seen to be large, often >50% of the 13:45 local time value. The spatial distribution of *RDV* is similar to that of *ADV* shown in Fig. 5, but in this case, illustrates the percentage diurnal uncertainties in emissions or
240 exposure that might be expected from assuming estimates based on LEO observations. As for the absolute diurnal variation, because this quantity depends on the number of useful cloud-free retrievals during the day it again represents a lower bound on the TrC variation. There are also no values in locations such as Japan and India where there is no 13:45 local time observation. The apparent high variation over the Pacific Ocean is a result of normalizing by the relatively low NO$_2$ TrC values in this region.

245 The January 2023 monthly average of the GEMS NO$_2$ TrC *ADV* and *RDV* over the Northeast Asia region are shown in Figs. A1 and A2, respectively. In general, reduced winter photochemistry results in a smaller diurnal variation in January compared to June. However, over polluted regions, the *ADV* in NO$_2$ TrC has similar values due to the higher January TrC. A noticeable region of high absolute daily change is also seen in Cambodia which requires further investigation but may be explained by fires. The Fig. A2 *RDV* map coverage is limited because the 13:45 local time observation is only available
250 between longitudes 113° E and 132° E.

GEMS NO₂ percent variability (%)
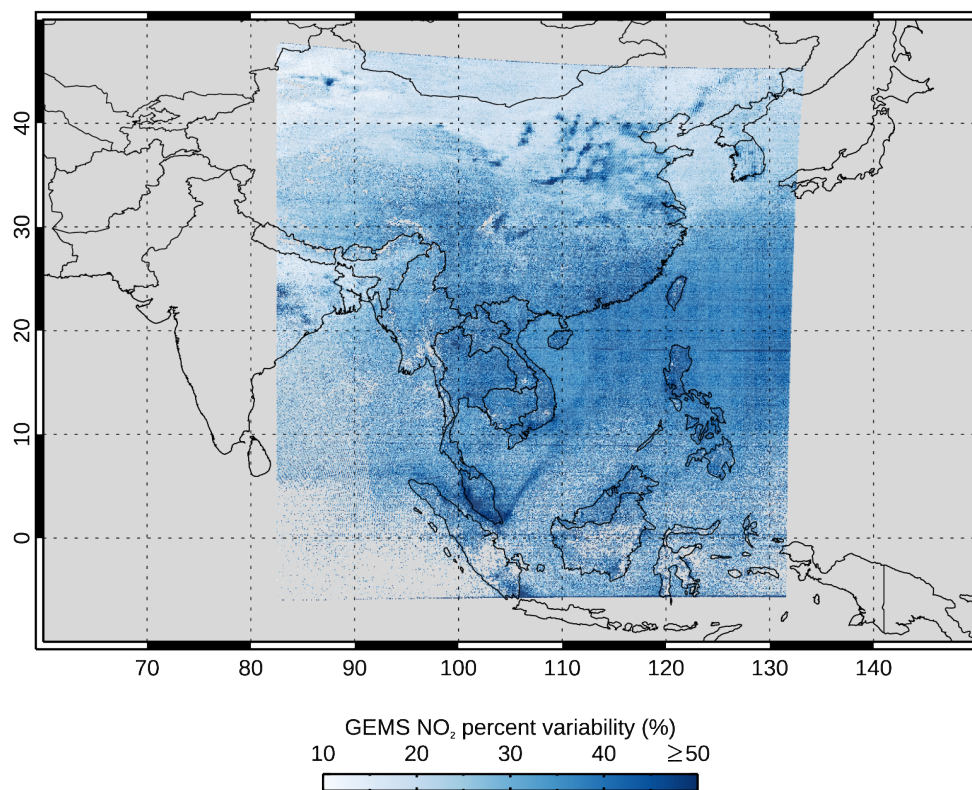
Figure 6: June 2023 monthly average of the GEMS NO₂ TrC relative daily variation (*RDV*) with respect to the 13:45 local time observed value at each location. Regions west of 90º E and east of ~130º E not mapped because there is no observation at 13:45 local time.

3.3 GEMS regional and local scale NO₂ diurnal variation time series

We have examined the time series of the GEMS NO₂ TrC for various regions and seasons. Fig. 7(a) shows the June 2023 time series spatially averaged over Northeast Asia (see Fig. 1 for regional context). At this time of year, there are a maximum of ten daylight hourly data points at the center of the GEMS FOR, fewer at the Eastern and Western edges. The number of hourly data points is further reduced by cloud filtering. Day-to-day, the calculated average TrC appears noisy because of the changing amount and nonuniformity of cloud-free coverage, especially when polluted urban areas might be included in the spatial average one day but not the next. Because of this, the monthly time-averaged diurnal variation (Fig. 7(b)) is the quantity often considered. However, it's important to show the individual daily TrC after filtering for cloudy data to indicate the information that will usually be available for AQ applications. It should also be noted that cloudy missing points in the daily data tends to 'flatten-out' the apparent diurnal variation shown in the monthly time average and suggests that this quantity be treated with care as it may not capture the full dynamic range of individual day diurnal variation.

Despite these considerations, a consistent diurnal cycle is seen on those days with multiple data points. This shows NO₂ TrC decreasing through the morning hours, reaching a minimum in the early afternoon, and then increasing again late in the afternoon. Little difference is seen between weekdays and weekends at this spatial scale. As discussed in Section 5, we attribute this summer cycle primarily to photochemistry being the dominant driver of diurnal variation since at this regional scale, diurnal variation due to different local-scale emissions and meteorology is averaged-out. This photochemical diurnal cycle is even more apparent when averaging over larger geographical regions although different local times, solar zenith angles and photolysis rates then complicate interpretation. A similar diurnal cycle is also seen in clean regions away from local sources or transported pollution plumes.
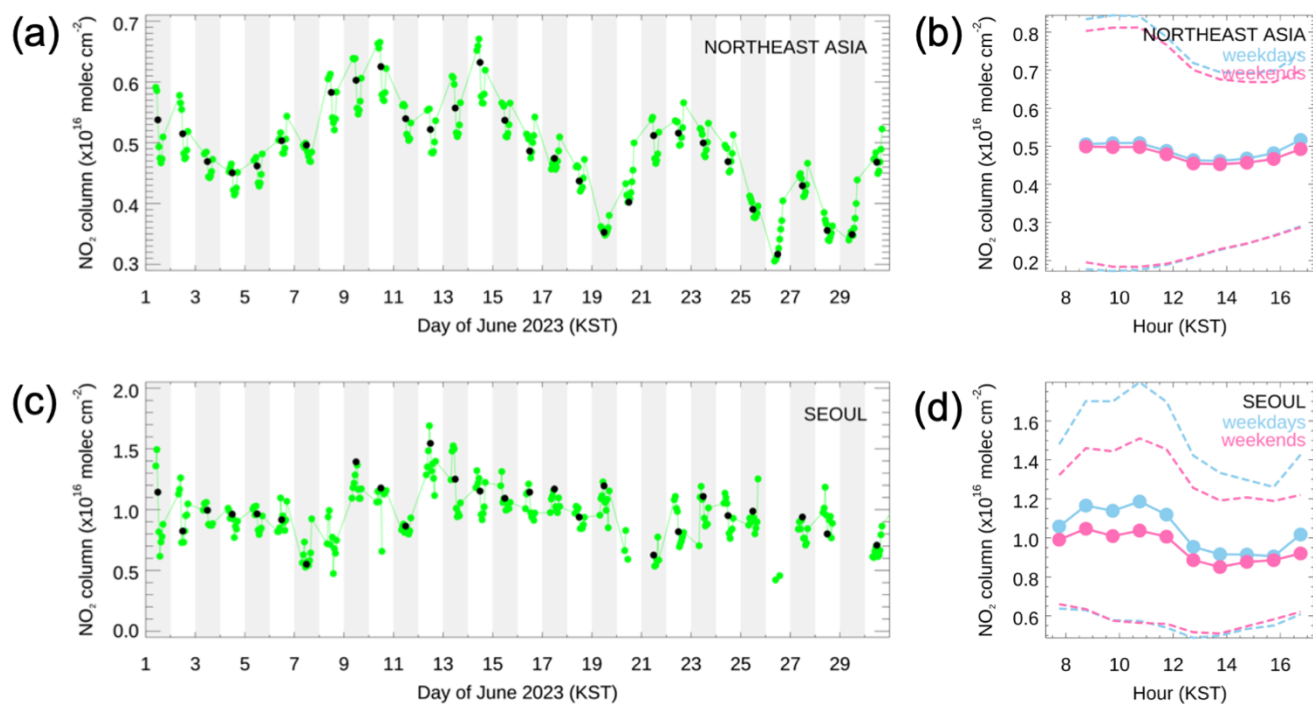
Figure 7: June 2023 diurnal NO₂ TrC values spatially averaged over (a) the Northeast Asia region, and (c) Seoul (see Fig. 1 for regional context). Depending on cloud cover, there are up to 10 data points each day and no data at night. The black dot each day indicates the value closest to local noon. The monthly-average weekday and weekend daily NO₂ variation is also shown for (b) the Northeast Asia region, and (d) Seoul. Note the high standard deviation (dashed lines).

The NO₂ diurnal variation is less consistent at local scale where, in addition to photochemistry, changing emissions and, more importantly, meteorology determine day-to-day variability. Fig. 7(c) shows the time series spatially averaged over Seoul, South Korea (126°–127.5° E, 37°–38° N; see Fig. 1 for regional context). Prior to the launch of GEMS, stagnation events over Seoul had been seen to cause build-up of pollution during the day leading to an afternoon maximum in NO₂ TrC.

This was observed by the Geostationary Trace gas and Aerosol Sensor Optimization (GeoTASO) aircraft spectrometer (Leitch et al., 2014) during the KORUS-AQ field campaign (Judd et al., 2018; Crawford et al., 2021). GEMS observations
285   sometimes show this same diurnal pattern, but as discussed in Section 5, more often show a photochemical 10:00-11:00 morning maximum in NO$_2$ contributed by urban emissions followed by a decrease and a small late afternoon increase as shown in the monthly time-averaged diurnal variation in Fig. 7(d). The weekend values indicate a similar diurnal cycle to weekdays with smaller TrC. We note that other work has shown large differences in the NO$_2$ diurnal variation seen by GEMS between weekdays and weekends for different Asian cities (Park et al., 2022a).

290   Reduced diurnal variation is shown in the January 2023 GEMS time series spatially averaged over the Northeast Asia and Seoul regions as shown in Fig. 8. As noted above, the apparent large day-to-day differences in TrC results primarily from the varying amount of cloud-free data that enter the spatial average, especially for the largescale Northeast Asia region. Over both regions, an increase in TrC is usually observed during the day because of reduced winter photochemistry as discussed in Section 5. This is the case for both weekdays and weekends although the weekday TrC values are now clearly greater
295   indicating the persistence of NO$_2$ resulting from higher weekday NO$_x$ emissions.
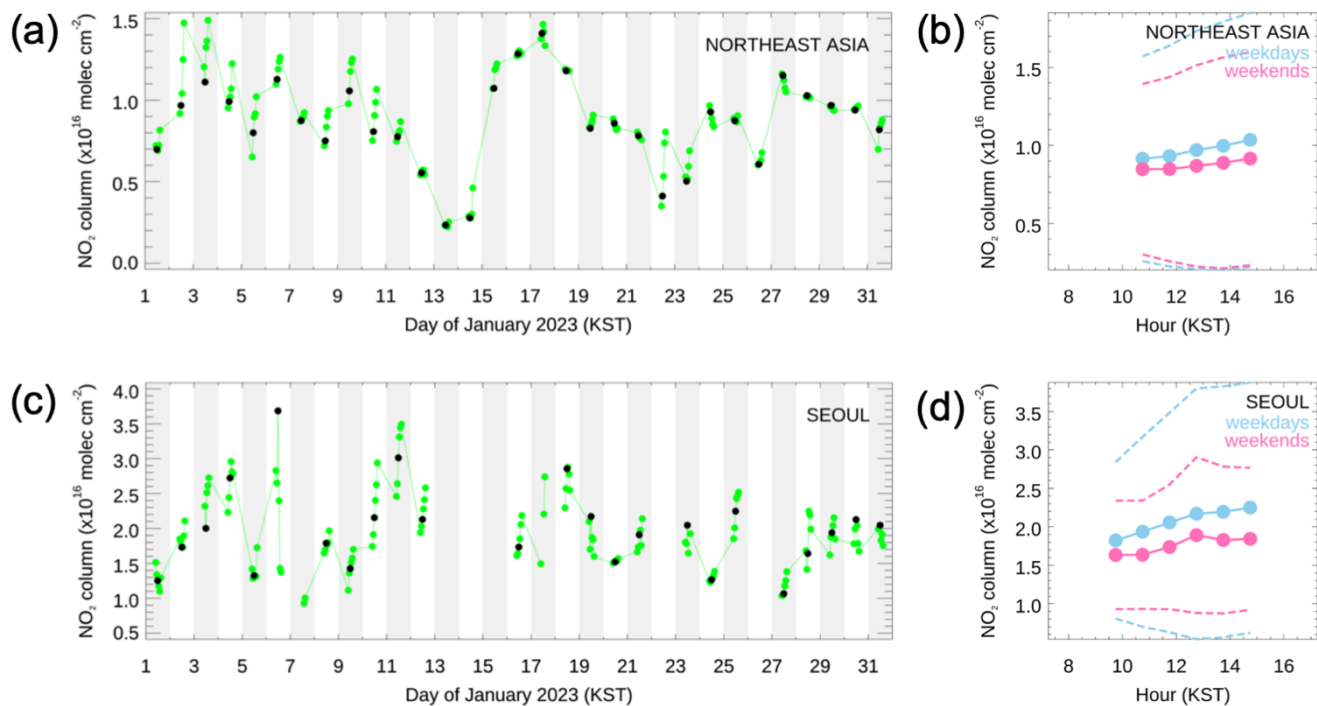
Figure 8: Same as Fig. 7 but now for January 2023 diurnal NO$_2$ TrC. Dependent on cloud cover, there are up to 6 data points each day and no data at night.

4 Pandora measurements in Seoul

300 The Pandora instruments have emerged as the primary source of ground-based measurements for validation of GEMS NO$_2$ and are also used extensively in TROPOMI validation (Kim et al., 2023). The advantage of these sun photometers is that they provide column retrievals using the same spectral bands as GEMS and have similar measurement vertical sensitivities. The number of Pandora stations across Asia has been rising rapidly and there are now 34 instruments contributing to the PGN. Here we use Pandora measurements in Seoul as an independent indication of the diurnal variation.

305 For our study months, there were two PGN Pandoras making measurements within Seoul, at Seoul National University (Seoul-SNU, Pandora#149) close to Mt. Gwanak, and about 12 km to the North across the city and closer to the center at Yonsei University (Seoul-YN, Pandora#54). A comparison of the monthly time-averaged diurnal variation of the NO$_2$ TotC measurements from GEMS and the Pandora instruments is shown in Fig. 9 for weekdays in June and January 2023. These also indicate the monthly mean TROPOMI TotC NO$_2$ at the local overpass time. We show Pandora NO$_2$ TotC retrievals that

310 use direct sun measurements rather than the Multi-Axis Differential Optical Absorption Spectroscopy (MAX-DOAS) measurements used for the TrC estimate. We also note that our model studies with the Whole Atmosphere Community Climate Model (WACCM) indicate that over relatively polluted regions such as Seoul, the stratosphere contributes only a few percent NO$_2$ to the total column. The GEMS and TROPOMI TotC are calculated using a mean of retrievals within 5 km of the Pandora sites. For the Pandora/satellite measurement comparisons we follow previous work (e.g., Judd et al., 2020;

315 Lambert et al., 2023).
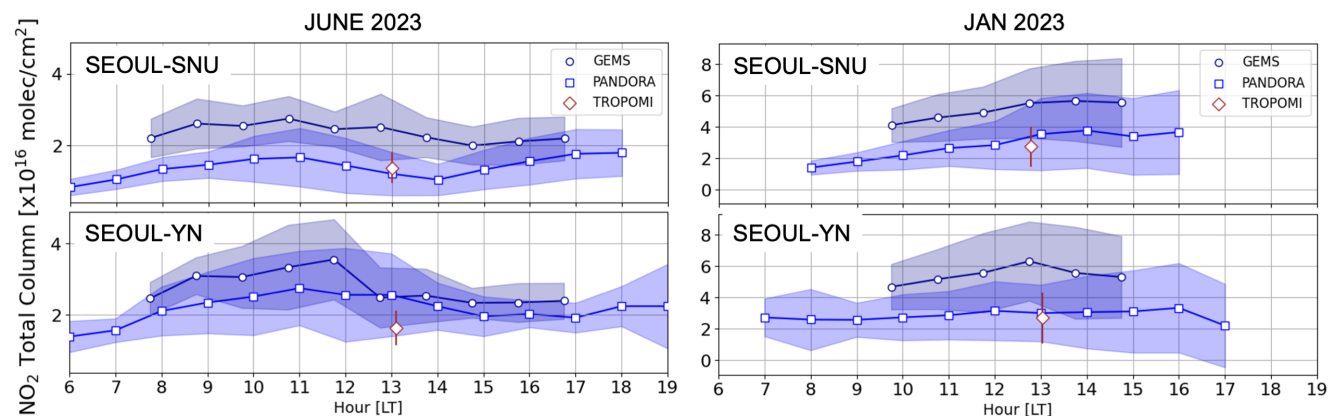
Figure 9: GEMS, TROPOMI, and Pandora NO$_2$ TotC values at Seoul-SNU and Seoul-YN, South Korea, for weekdays in June and January 2023. The GEMS and TROPOMI TotC are calculated using a mean of retrievals within 5 km of the Pandora sites.

The GEMS NO$_2$ TotC values are overall larger than their Pandora counterparts with a higher bias in January than June. This

320 positive bias has also been identified in comparisons with ground-based DOAS measurements with a median relative difference of +64 % and a correlation coefficient of 0.75 (Lange et al., 2024). This is contrary to what is usually found when

comparing pixel-averaged satellite retrievals to local measurements that might capture small-scale high values (e.g. Herman et al., 2019). Tang et al. (2021) show that this representativeness error can account for a single Pandora measurement in Seoul being as much as ~25% higher than the GEMS retrieval for the corresponding pixel. Indeed Kim et al. (2023) found that GEMS V1.0 NO$_2$ TotC measurements tend to be lower than their Pandora counterparts at less polluted sites south of Seoul. Our own analysis at other Korean Pandora sites shows a much lower GEMS/Pandora bias in clean regions along with a small or flat diurnal variation that was also reported by Lange et al., 2024. We find that the GEMS V2.0 data positive bias is less than that of the previous V1.0 data but may still indicate retrieval issues to be addressed in future GEMS data releases. (A limited preview of the upcoming GEMS V3.0 NO$_2$ data release with improved AMF calculation and StrC/TrC separation shows closer agreement with TROPOMI in summer but still an overestimation in winter.) The agreement between Pandora and TROPOMI is good at both sites and for both months, even though large negative (0 to -50%) biases in TROPOMI NO$_2$ TotC have previously been reported (Verhoelst et al., 2021). We note here that we find no obvious measurement local time dependence in the GEMS/Pandora bias for Seoul or for the other Korean sites that we have examined.

Despite the positive GEMS bias, the agreement in pattern of NO$_2$ TotC diurnal variation captured by the Pandoras and the corresponding GEMS observations is reasonable at both Seoul sites in both months. The column amounts are lower in June than in January and indicate a morning NO$_2$ maximum followed by a decrease through early afternoon and then a slight increase in the late afternoon. A clear rush-hour peak is not seen in these TotC measurements and is discussed further in Section 5.2. The sharp gradient in GEMS data over Seoul-YN in June between 12:00 and 13:00 is due to the value at 13:00 being anomalously low. This occurs because of the limited number of measurements (2-3 per day) that meet the coincidence criteria with Pandora and then the low number of cloud-free days in this month. The weekend values (not shown) have a flatter diurnal profile and less variation within each hour, though the average magnitude is only slightly smaller than weekdays. In January, both sites show a flat or increasing TrC during the day.

The Pandora NO$_2$ TotC are generally higher at Seoul-YN in June under the prevailing wind from the South at this time of year that blows more pollution from the city center toward this Pandora site. The opposite occurs during January when the prevailing wind is from the Northeast. The same finding for Pandora/TROPOMI comparisons was previously reported by Park et al. (2022b). The GEMS satellite data captures some of this difference between the two sites and suggests more work is needed to assess the capability the of GEMS to resolve pixel-scale urban variability for AQ applications.

5 Model studies and discussion

5.1 Model NO$_2$ diurnal variation

350 We have used the MUSICAv0 model to simulate the NO₂ TrC for the same Northeast Asia and Seoul regions discussed above for June and January of 2023, and the model setup was as described in Section 2.4. For each case, we performed two simulations as a sensitivity test to the assumed anthropogenic diurnal emissions profile. The first assumes constant anthropogenic emissions during the day (labeled Base), the second uses the KORUS-AQ area/point and mobile sector diurnal emissions profiles described in Section 2.4 and shown in Fig. 2 (labeled Diurnal). The average daily NO₂ TrC diurnal

355 variation for weekdays is shown in Fig. 10. The time windows corresponding to the periods during which GEMS retrievals are shown in Figs. 7 and 8 are indicated by the unshaded hours. As was noted in Section 2.4, there is an issue with the GEMS V2.0 NO₂ averaging kernels which should not be used following the guidance of NIER. As a result, the discussion here comparing MUSICAv0 simulations to the GEMS retrievals presented in Section 3.3 should be considered as mainly qualitative. However, we believe that the model is still able to provide insights into the drivers of the NO₂ TrC diurnal

360 variation and that presentation of these results is worthwhile as it sets the stage for more quantitative analysis with the next GEMS data version.
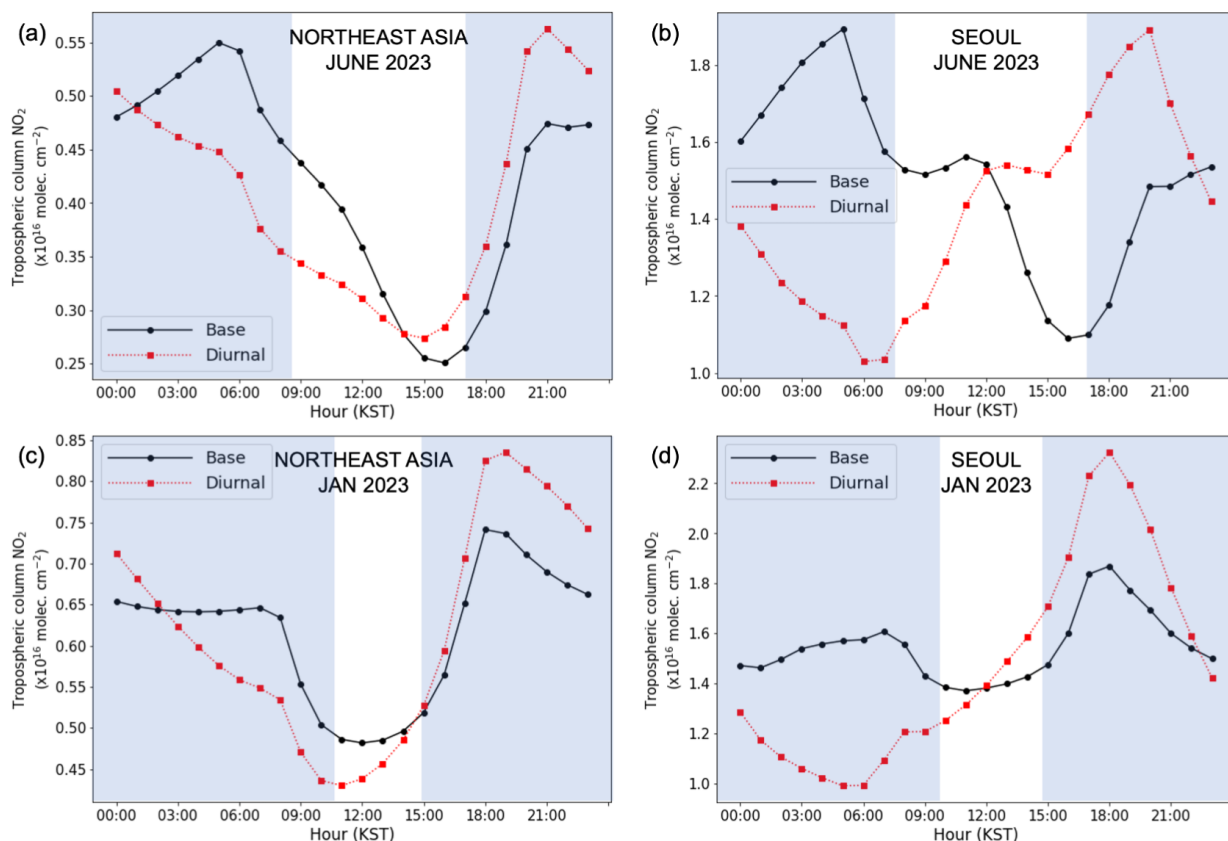
Figure 10: MUSICAv0 NO₂ TrC diurnal variation averaged over the Northeast Asia region (left) and Seoul (right) for weekdays in June 2023 (top row) and January 2023 (bottom row). The time windows corresponding to the periods during which GEMS retrievals are shown in Figs. 7 and 8 are indicated by the unshaded hours. The Base simulation assumes a

constant diurnal emissions profile, the Diurnal simulation uses the diurnal emissions profile discussed in Section 2.4 and shown in Fig. 2.

5.2 The role of emissions

We first consider the model results spatially averaged over the Northeast Asia study region and temporally averaged for weekdays in the months of June and January 2023, Fig 10 (a) and (c), respectively. The model patterns for the NO_2 TrC diurnal variation are in general similar to the corresponding GEMS Figs. 7(b) and 8(b). However, since the model does not include cloud cover and reproduces a consistent daily pattern, the dynamic range of the diurnal variation is greater than the averaged GEMS data. The GEMS data are biased high relative to the model in both months with the difference being largest in January. This may be a GEMS V2.0 retrieval issue as noted above and/or an underestimation of NO_x emissions in MUSICAv0. At this regional scale, the diurnal variation is similar for both the Base and Diurnal simulations despite the very different anthropogenic diurnal emissions profiles and suggests that photochemistry is the main driver. However, the magnitude of the diurnal variation during the GEMS retrieval window does depend on the emissions profile, ranging from 25-50% in June to 6-17% in January. We note the GEMS NO_2 TrC daily relative variation over Northeast Asia for June and January 2023 (Figs. 6 and A2, respectively) falls at the bottom of these ranges suggesting further work is needed to understand the greater model variation. The emissions profile also affects the local hour of the minimum NO_2 TrC and is about an hour earlier in the Diurnal case which matches better with GEMS.

Over the Seoul region, the difference in NO_2 diurnal variation between the Base and Diurnal simulations is large, especially in June (Fig. 10(b)). For the Base simulation in June, the shape of the diurnal variation shows a similar photochemical cycle as described above for the Northeast Asia region. A difference is seen in that there is a NO_2 morning peak around 10:00-11:00 before the decrease through midday to an afternoon minimum and is like the diurnal variation seen in the corresponding GEMS data (Fig. 7(d)). This is discussed further in the next Section. In contrast, the Diurnal simulation shows a very different NO_2 build-up throughout the day and reflects the shape of the NO_x diurnal emissions profile used in the model, although the pronounced rush-hour peaks seen in Fig. 2 are not evident in the NO_2 TrC average even though they do clearly show up in the calculated surface concentration (not shown). However, the fact that the average GEMS NO_2 diurnal variation shown in Fig. 7(d) more closely resembles the constant NO_x emissions of the Base simulation suggests that the hourly changes in the emissions profile may not actually be as large as indicated in Fig. 2. In January, both simulations show increasing TrC during the GEMS retrieval window in agreement with the GEMS data in Fig 8(d). These simulations indicate that the modeled diurnal variation at the city scale will be very dependent on the assumed emissions diurnal profile, accurate characterization of which will be an important part of effectively using the hourly observations from GEO.

5.3 The role of chemistry

The underlying photochemical cycle is explained by considering the June 2023 Base simulation TrC NO_x budget analysis

shown in Fig. 11(a) for Seoul. After build-up of NO_2 during nighttime, photolysis begins with sunrise at 05:00 and the morning decrease is mirrored by the increase in NO with the rise of the NO_2 photolysis rate (j_{NO2}) curve with increasing solar elevation. Although the NO_x ratio is in photochemical steady state on timescales of minutes, the diurnal change in solar irradiance drives a continual change in the ratio through the day. It should also be remembered that this calculation is for the

400   TrC relevant to the GEMS retrieval and is therefore representative of a vertically weighted average rather than surface values. After 10:00, NO loss with the build-up of O_3 pushes the NO_x ratio toward NO_2 at the same time that NO_x is lost to nitrogen reservoirs HNO_3, and to a lesser extent, PAN. This balance results in a slight peak in NO_2 around 11:00 before a continued decline due to NO_x loss until the minimum at 16:00. Decreasing photolysis results in a subsequent NO_2 increase into nighttime with continuing NO_x emissions. The underlying chemistry is similar for the corresponding June Diurnal

405   simulation (not shown) only in this case, the increasing NO_x emissions during the day result in replacement of most of the atmospheric NO_x that is lost to the nitrogen reservoirs with a consequent gradual buildup of NO_2.

In the January 2023 Base simulation shown in Fig. 11(b), atmospheric NO_x shows less variation under conditions of lower photolysis, lower O_3, and less daytime conversion to HNO_3. The NO_x ratio depends mainly on the change in the j_{NO2} curve under conditions of limited photochemical activity resulting in a 11:00 maximum in NO and minimum in NO_2 (as shown in

410   Fig. 10(d)). In the January Diurnal simulation (not shown), NO_2 again builds up during the day following the increasing NO_x emissions.
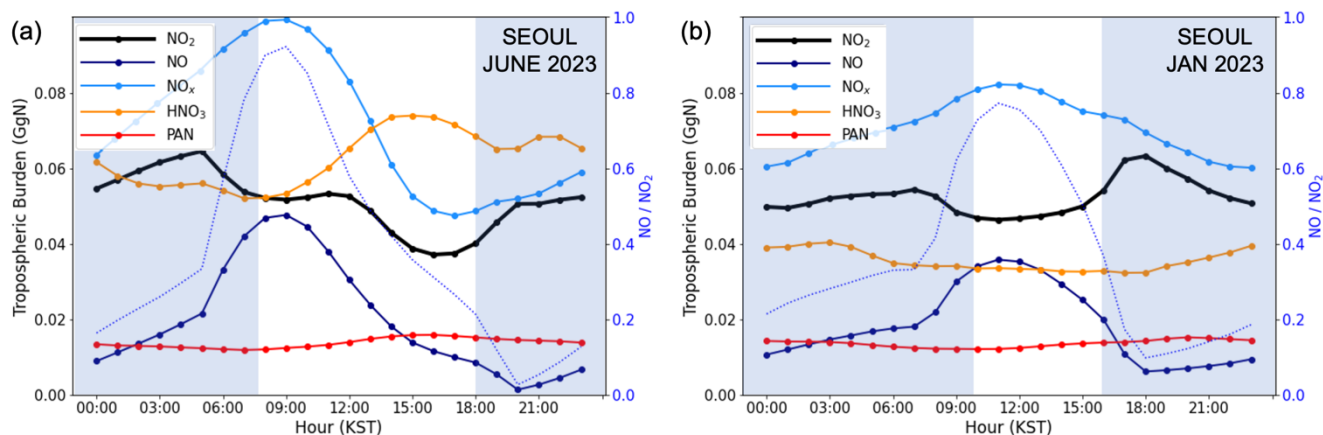
Figure 11: MUSICAv0 (a) June and (b) January 2023 average daily NO_x TrC budget analysis over Seoul. Constant anthropogenic emissions during the day (Base simulation). The time windows corresponding to the periods during which

415   GEMS retrievals are shown in Figs. 7 and 8 are indicated by the unshaded hours.

5.4 The role of meteorology

The MUSICAv0 average daily NO_2 TrC diurnal variation averaged over Seoul (shown in Figs. 10(b) and (d)) results from averaging the diurnal variation during each day of June and January 2023. As noted before, the Base simulation usually

shows an afternoon minimum whereas the Diurnal simulation shows a build-up of pollution during the day producing a late
420 afternoon NO_2 peak. Both simulations indicate that day-to-day changes in NO_2 TrC magnitude depend primarily on meteorology. This is illustrated in Fig. 12 which shows the correlation of the average model NO_2 TrC during the day with the model surface layer wind (usually around ~120 m) and also indicates the average wind direction over the city. This is shown separately in plots for June and January calculations for the two years 2022 and 2023 together. For both months, there is a clear anticorrelation (R about -0.7) of NO_2 TrC and wind speed. In June, the prevailing wind over Seoul is usually from
425 the South. Shifts to the winds from the West results in lower wind speed and stagnant conditions over the city that permit a build-up of pollution, and this is reflected in the TrC value. Similar anticorrelation is seen in January, although during winter the winds over Seoul are mostly from the Northwest and an occasional change to a weak anticyclonic pattern results in low wind speed and NO_2 TrC buildup.
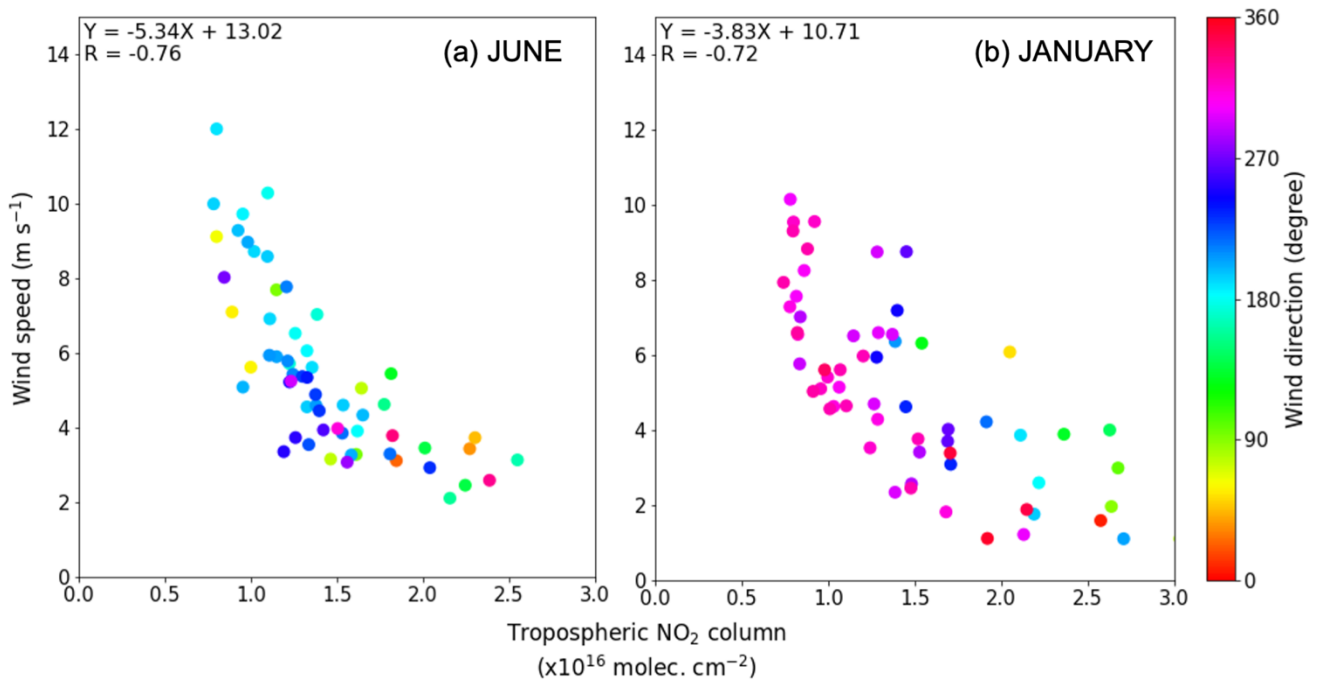
430 **Figure 12:** Scatterplot of the MUSICAv0 average daily NO_2 TrC compared to the magnitude and direction of the prevailing model surface layer wind (usually around ~120 m) over Seoul for June and January combined data for in the two years 2022 and 2023. Constant anthropogenic emissions during the day (Base case).

A similar analysis for the modeled diurnal variation absolute daily change in NO_2 TrC discussed in Section 3.2 does not show clear correlation (R about -0.35) with wind speed in either month over Seoul. This suggests that the emission and

chemistry processes discussed above are most important in determining the local diurnal variation and do not necessarily require stagnant meteorological conditions. We note that Yang et al (2023b) did see correspondence between low model wind speed and higher winter NO_2 diurnal variation, so further investigation would be useful using wind measurements. We have also examined the contribution of incoming transport to the NO_2 TrC, although Seoul is unlikely to be a generally representative city in this respect as it is large, fairly isolated, and has very high local NO_x emissions. Upwind GEMS NO_2 TrC values are usually about 3–4 times lower than the values retrieved over the city and have relatively flat diurnal variation, suggesting incoming transport contributions to the Seoul NO_2 TrC diurnal or day-to-day variations will be small. This might not be the case for longer lived pollutants or when considering concentrations at a specific altitude such as in the free troposphere (Jordan et al., 2020). In cleaner regions downwind of Seoul, the GEMS NO_2 TrC do show higher values because of plumes following a high pollution day over the city. Understanding the role of meteorology is going to be important for our next step of relating the satellite retrievals of TrC to surface concentrations. Results from KORUS-AQ showed that meteorology and PBL dynamics play a large role in determining the extent to which the satellite and ground-based in situ views of pollutant diurnal variation can be reconciled (Crawford et al., 2021).

6 Conclusion

Over the last 20 years, LEO observations have provided satellite measurements of pollutants in the atmosphere with increasing scientific utility, mainly at continental-to-global, weekly-to-seasonal scales. New-generation LEO instruments (e.g., IASI, CrIS, and TROPOMI) have allowed for refinements in both spatial and temporal resolution, to city- and daily-scales. The GEO satellite perspective, with hourly high spatial resolution measurements, represents another major step forward, especially in capabilities for understanding how AQ processes change diurnally at the local scale. The main conclusions of this work are:

1. GEMS observations show that NO_2 TrC diurnal variation can be large (>50% of the TrC) and varies by location, being higher in polluted environments. The NO_2 distribution is seen to change hourly and can be quite different from what would be seen in a once-a-day LEO observation. This is demonstrated by the quantitative measures of diurnal variation that we have presented such as the monthly average of the absolute daily change in TrC or the diurnal relative variation in TrC. Along with enabling one or more observations within a day under changing cloud conditions, this demonstrates the advantages of the GEO perspective.

2. Regionally averaging GEMS NO_2 TrC data emphasizes the diurnal variation due to chemistry since local scale variability due to emissions and meteorology is minimized. Temporally averaging the data hourly emphasizes persistent chemistry and emissions patterns while minimizing meteorological variability.

3. In June, NO_2 photochemistry is an important driver of diurnal variation, especially at the regional scale. At local scale, NO_2 magnitude and diurnal variation patterns change day-to-day, showing the impact of emissions and meteorology. In

January, NO$_2$ columns are higher and diurnal variation is lower because of reduced photochemistry.

4. Initial comparisons with Pandora measurements over Seoul show a reduction in GEMS V2.0 positive bias with respect to GEMS V1.0 and reasonable agreement on the shape of diurnal variation. The GEMS differences between the two Pandora sites suggests the possibility of resolving pixel-scale urban variation for AQ applications.

470 5. Model simulations show high sensitivity to the assumed diurnal emissions profile, especially at local scale. This will have consequences ranging from the assumed NO$_2$ vertical profile used in retrieval AMF calculations to the background model field used for GEMS data assimilation.

6. The model indicates an anticorrelation between the surface layer wind speed and the daily mean NO$_2$ TrC which can build up under stagnant conditions.

475 This work has concentrated on understanding the diurnal variation of the GEMS NO$_2$ TrC retrievals with a CTM. In combination with ground-based remote sensing and in situ measurements, the next step will be to connect the GEO and LEO satellite-derived columns (not only of NO$_2$ but also other trace gas species, particularly O$_3$ and HCHO) to the surface level concentrations. This will allow derivation of top-down diurnal emissions profiles that can be applied to the standard bottom-up emissions inventories. Including this diurnal variation is going to be important for determining true pollutant exposure

480 levels for AQ studies. The work presented here also provides a path for investigating similar NO$_2$ diurnal cycles in the new TEMPO data over North America, and later over Europe with S-4.

485

Appendix A
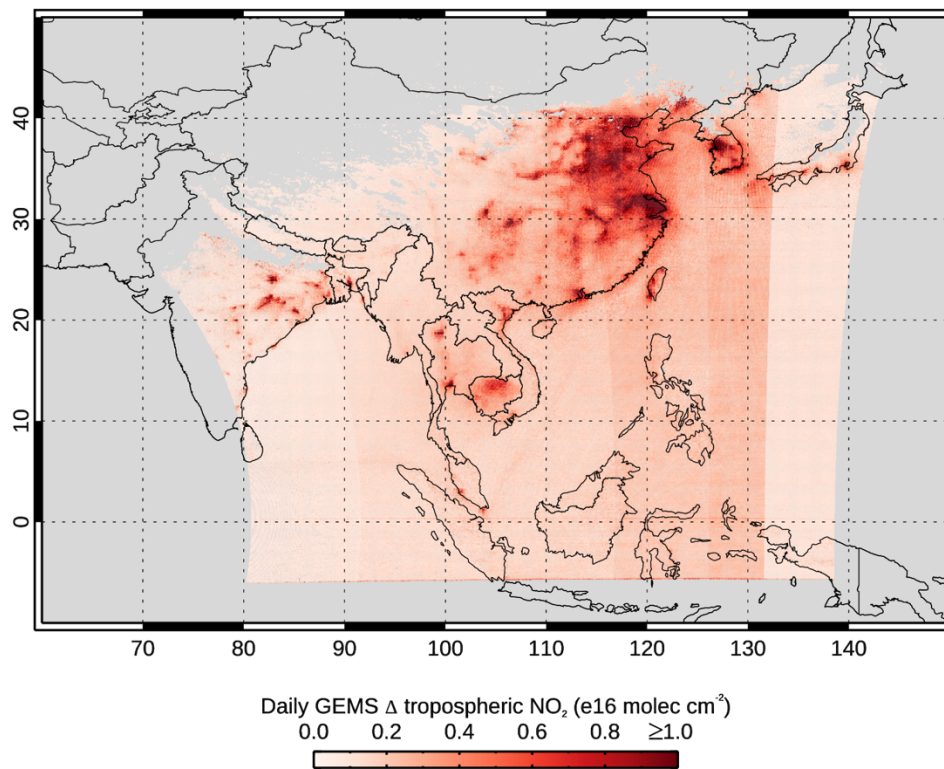
Figure A1: Monthly average of the absolute daily variation (*ADV*) in the GEMS NO₂ TrC for January 2023. Data points with 3 or more observations per day were included in this analysis.
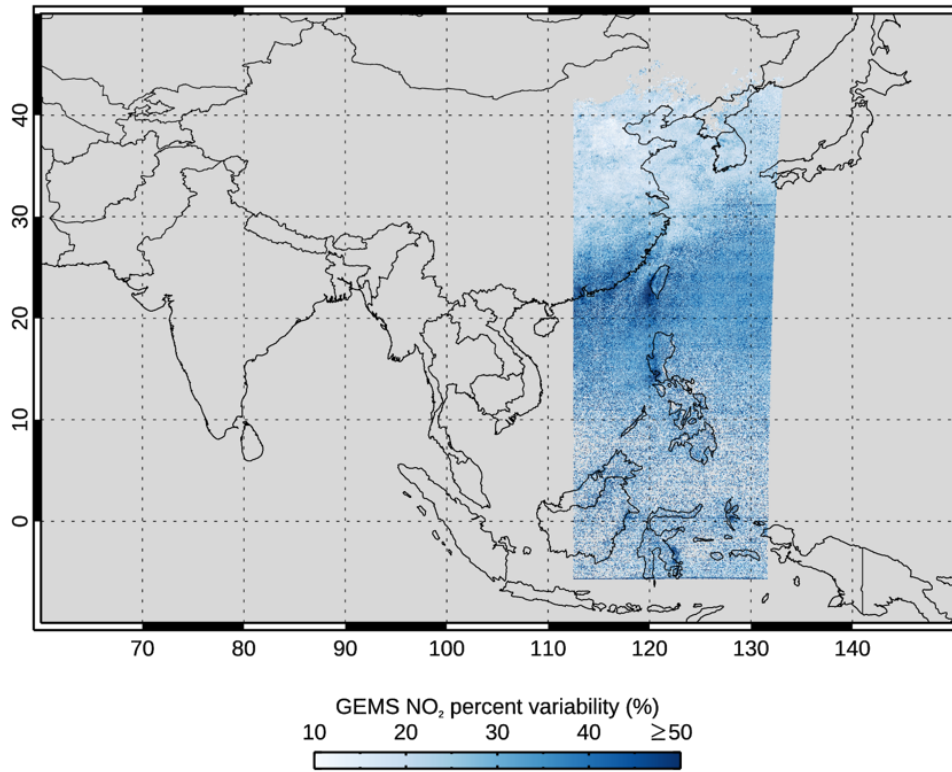
Figure A2: January 2023 monthly average of the GEMS NO₂ TrC relative daily variation (*RDV*) with respect to the 13:45 local time observed value at each location. Regions west of about 113° E and east of about 132° E are not mapped due to lacking observations at 13:45 local time.

Competing interests

At least one of the (co-)authors is a member of a Copernicus journal editorial board.

Acknowledgement

This work was partly supported by Smithsonian Institution subcontract SV3-83021. This material is based upon work supported by the National Center for Atmospheric Research, which is a major facility sponsored by the National Science Foundation under Cooperative Agreement No. 1852977. We would like to acknowledge high-performance computing support from Cheyenne (doi:10.5065/D6RX99HX) provided by NSF NCAR's Computational and Information Systems Laboratory, sponsored by the National Science Foundation. We thank Doug Kinnison (NCAR/ACOM) for providing WACCM simulations and discussing stratospheric NO_2. We thank the TROPOMI and PGN teams for observational data.

Author contribution

Conceptualization, DPE; Methodology, DPE, SMA, DSJ, and IO; Formal analysis, DPE, SMA, DSJ, and IO; Data curation, SMA, DSJ, IO, HL, JP, and HH; Validation, SMA, IO, JK, HL, JP, and HH; Visualization, SMA, DSJ, and IO; Supervision, DPE, HMW, and LKE; Writing – original draft preparation, DPE and SMA; Writing – review & editing, SMA, DSJ, IO, LKE, JJO, HMW, JK, HL, JP, and HH.

Data availability

The GEMS L2 NO_2 V2.0 data can be obtained on application to NIER (https://nesc.nier.go.kr/en/html/cntnts/91/static/page.do). The Pandora NO_2 data are available from the Pandonia Global Network data archive (http://data.pandonia-global-network.org/). The TROPOMI NO_2 data are publicly available from the NASA Earthdata portal (https://search.earthdata.nasa.gov/).

Code availability

MUSICAv0 is a configuration of CESM2.2, which is an open-source community model available from: https://github.com/ESCOMP/CESM. The code modifications for including diurnal cycle of anthropogenic emissions, grid information files, and simulation results are available at [https://doi.org/10.5281/zenodo.8044736].

References

Bazalgette Courrèges-Lacoste, G., Sallusti, M., Bulsa, G., Bagnasco, G., Veihelmann, B., Riedl, S., Smith, D. J., and Maurer, R.: The Copernicus Sentinel 4 mission: A geostationary imaging UVN spectrometer for air quality monitoring, Proc. SPIE 10423, Sensors, Systems, and Next-Generation Satellites XXI, 10423, https://doi.org/10.1117/12.2282158, 2017.

Beirle, S.: Estimate of nitrogen oxide emissions from shipping by satellite remote sensing, Geophysical Research Letters, 31, https://doi.org/10.1029/2004gl020312, 2004.

Bey, I., Jacob, D. J., Yantosca, R. M., Logan, J. A., Field, B., Fiore, A. M., Li, Q., Liu, H., Mickley, L. J, .and Schultz, M.: Global modeling of tropospheric chemistry with assimilated meteorology: Model description and evaluation, J. Geophys. Res., 106, 23,073-23,096, 2001.

Boersma, K. F., Vinken, G. C. M., and Eskes, H. J.: Representativeness errors in comparing chemistry transport and chemistry climate models with satellite UV–Vis tropospheric column retrievals, Geosci. Model Dev., 9, 875–898, 10.5194/gmd-9-875-2016, 2016.

Brasseur, G., Orlando, J. J., and Tyndall, G. S. (Eds.): Atmospheric chemistry and global change, Oxford University Press, New York, ISBN: 9780195105216, 1999.

Bucsela, E. J., Krotkov, N. A., Celarier, E. A., Lamsal, L. N., Swartz, W. H., Bhartia, P. K., Boersma, K. F., Veefkind, J. P., Gleason, J. F., and Pickering, K. E.: A new stratospheric and tropospheric NO2 retrieval algorithm for nadir-viewing satellite instruments: applications to OMI, Atmos. Meas. Tech., 6, 2607-2626, 10.5194/amt-6-2607-2013, 2013.

CEOS: A geostationary satellite constellation for observing global air quality: An international path forward, CEOS atmospheric composition constellation executive summary, https://ceos.org/observations/documents/AC-VC_Geostationary-Cx-for-Global-AQ-final_Apr2011.pdf, 2019.

Choi, Y., Kim, G., Kim, B. and Kwon, M.: Geostationary Environment Monitoring Spectrometer (GEMS) algorithm theoretical basis document cloud retrieval algorithm Ministry of Environment. Retrieved from https://nesc.nier.go.kr/en/html/satellite/doc/doc.do, 2020.

Clerbaux, C., Boynard, A., Clarisse, L., George, M., Hadji-Lazaro, J., Herbin, H., Hurtmans, D., Pommier, M., Razavi, A., Turquety, S., Wespes, C., and Coheur, P.-F.: Monitoring of atmospheric composition using the thermal infrared IASI/MetOp sounder, Atmospheric Chemistry and Physics, 9, 6041–6054, https://doi.org/10.5194/acp-9-6041-2009, 2009.

Crawford, J. H., Ahn, J.-Y., Al-Saadi, J., Chang, L., Emmons, L. K., Kim, J., Lee, G., Park, J.-H., Park, R. J., Woo, J. H.,

545 Song, C.-K., Hong, J.-H., Hong, Y.-D., Lefer, B. L., Lee, M., Lee, T., Kim, S., Min, K.-E., Yum, S. S., and Shin, H. J.: The Korea–United States Air Quality (KORUS-AQ) field study, Elementa: Science of the Anthropocene, 9, https://doi.org/10.1525/elementa.2020.00163, 2021.

Crippa, M., Solazzo, E., Huang, G., Guizzardi, D., Koffi, E., Muntean, M., Schieberle, C., Friedrich, R., and Janssens-Maenhout, G.: High resolution temporal profiles in the Emissions Database for Global Atmospheric Research, Scientific 550 Data, 7, https://doi.org/10.1038/s41597-020-0462-2, 2020.

Curier, R. L., Kranenburg, R., Segers, A. J. S., Timmermans, R. M. A., and Schaap, M.: Synergistic use of OMI NO2 tropospheric columns and LOTOS–EUROS to evaluate the NOx emission trends across Europe, Remote Sensing of Environment, 149, 58-69, https://doi.org/10.1016/j.rse.2014.03.032, 2014.

de Foy, B. and Schauer, J. J.: An improved understanding of NO_x emissions in South Asian megacities using TROPOMI 555 NO_2 retrievals, Environmental Research Letters, 17, 024006, https://doi.org/10.1088/1748-9326/ac48b4, 2022.

Earthdata NASA portal, https://search.earthdata.nasa.gov/, last access: 14 February 2024.

deRuyter de Wildt, M., Eskes, H., and Boersma, K. F.: The global economic cycle and satellite-derived NO_2 trends over shipping lanes, Geophys. Res. Lett., 39, L01802, doi:10.1029/2011GL049541, 2012.

Duncan, B., Yoshida, Y., de Foy, B., Lamsal, L., Streets, D., Lu, Z., Pickering, K., and Krotkov, N.: The observed response 560 of Ozone Monitoring Instrument (OMI) NO_2 columns to NO_x emission controls on power plants in the United States: 2005–2011, Atmos. Environ., 81, 102–111, doi:10.1016/jatmosenv.2013.08.068, 2013.

Duncan, B. N., Lamsal, L. N., Thompson, A. M., Yoshida, Y., Lu, Z., Streets, D. G., Hurwitz, M. M., Pickering, K.R.: A space-based, high-resolution view of notable changes in urban NOx pollution around the world (2005–2014), Journal of Geophysical Research: Atmospheres, 121,2,976-996, https://doi.org/10.1002/2015JD024121, 2016.

565 Emmons, L. K., Schwantes, R. H., Orlando, J. J., Tyndall, G., Kinnison, D., Lamarque, J., Marsh, D., Mills, M. J., Tilmes, S., Bardeen, C., Buchholz, R. R., Conley, A., Gettelman, A., García, R., Simpson, I., Blake, D. R., Meinardi, S., and Pétron, G.: The Chemistry Mechanism in the Community Earth System Model Version 2 (CESM2), Journal of Advances in Modeling Earth Systems, 12, https://doi.org/10.1029/2019ms001882, 2020.

Fishman, J., Iraci, L. T., Al-Saadi, J., Chance, K., Chavez, F., Chin, M., Coble, P., Davis, C., DiGiacomo, P. M., Edwards, 570 D., Eldering, A., Goes, J., Herman, J., Hu, C., Jacob, D. J., Jordan, C., Kawa, S. R., Key, R., Liu, X., and Lohrenz, S.: The United States' next generation of atmospheric composition and coastal ecosystem measurements: NASA's GEOstationary Coastal and Air Pollution Events (GEO-CAPE) mission, Bulletin of the American Meteorological Society, 93, 1547–1566, https://doi.org/10.1175/BAMS-D-11-00201.1, 2012.

Franke, K., Richter, A., Bovensmann, H., Eyring, V., Jöckel, P., Hoor, P., and Burrows, J. P.: Ship emitted NO_2 in the Indian Ocean: Comparison of model results with satellite data, Atmospheric Chemistry and Physics, 9, 7289–7301, https://doi.org/10.5194/acp-9-7289-2009, 2009.

Geddes, J. A., Martin, R. V., Bucsela, E. J., McLinden, C. A., and Cunningham, D. J. M.: Stratosphere–troposphere separation of nitrogen dioxide columns from the TEMPO geostationary satellite instrument, Atmospheric Measurement Techniques, 11, 6271–6287, https://doi.org/10.5194/amt-11-6271-2018, 2018.

Georgoulias, A. K., Boersma K. F., van Vliet, J., Zhang, X., van der A, R., Zanis, P., and de Laat, J.: Detection of NO_2 pollution plumes from individual ships with the TROPOMI/S5P satellite sensor, Environmental Research Letters, 15, 124037–124037, https://doi.org/10.1088/1748-9326/abc445, 2020.

Goldberg, D. L., Anenberg, S. C., Kerr, G. H., Mohegh, A., Lu, Z., and Streets, D. G.: TROPOMI NO_2 in the United States: A detailed look at the annual averages, weekly cycles, effects of temperature, and correlation with surface NO_2 concentrations, Earth's Future, 9, https://doi.org/10.1029/2020ef001665, 2021.

Griffin, D., McLinden, C. A., Dammers, E., Adams, C., Stockwell, C. E., Warneke, C., Bourgeois, I., Peischl, J., Ryerson, T. B., Zarzana, K. J., Rowe, J. P., Volkamer, R., Knote, C., Kille, N., Koenig, T. K., Lee, C. F., Rollins, D., Rickly, P. S., Chen, J., and Fehr, L.: Biomass burning nitrogen dioxide emissions derived from space with TROPOMI: methodology and validation, Atmospheric Measurement Techniques, 14, 7929–7957, https://doi.org/10.5194/amt-14-7929-2021, 2021.

Griffin, D., Zhao, X., McLinden, C. A., Boersma, F., Bourassa, A., Dammers, E., Degenstein, D., Eskes, H., Fehr, L., Fioletov, V., Hayden, K., Kharol, S. K., Li, S., Makar, P., Martin, R. V., Mihele, C., Mittermeier, R. L., Krotkov, N., Sneep, M., and Lamsal, L. N.: High-resolution mapping of nitrogen dioxide with TROPOMI: First results and validation over the Canadian Oil Sands, Geophysical Research Letters, 46, 1049–1060, https://doi.org/10.1029/2018gl081095, 2019.

Guenther, A. B., Jiang, X., Heald, C. L., Sakulyanontvittaya, T., Duhl, T., Emmons, L. K., and Wang, X.: The Model of Emissions of Gases and Aerosols from Nature version 2.1 (MEGAN2.1): An extended and updated framework for modeling biogenic emissions, Geoscientific Model Development, 5, 1471–1492, https://doi.org/10.5194/gmd-5-1471-2012, 2012.

Han, Y., Revercomb, H., Cromp, M., Gu, D., Johnson, D., Mooney, D., Scott, D., Strow, L., Bingham, G., Borg, L., Chen, Y., DeSlover, D., Esplin, M., Hagan, D., Jin, X., Knuteson, R., Motteler, H., Predina, J., Suwinski, L., and Taylor, J.: Suomi NPP CrIS measurements, sensor data record algorithm, calibration and validation activities, and record data quality, Journal of Geophysical Research: Atmospheres, 118, 12, 734–12, 748, https://doi.org/10.1002/2013jd020344, 2013.

Herman, J. R., Cede, A., Spinei, E., Mount, G. H., Tzortziou, M., and Nader Abuhassan: NO_2 column amounts from ground-

based Pandora and MFDOAS spectrometers using the direct-sun DOAS technique: Intercomparisons and application to OMI validation, Journal of Geophysical Research, 114, https://doi.org/10.1029/2009jd011848, 2009.

Herman, J., Abuhassan, N., Kim, J., Kim, J., Dubey, M., Raponi, M., and Tzortziou, M.: Underestimation of column NO2
605 amounts from the OMI satellite compared to diurnally varying ground-based retrievals from multiple PANDORA spectrometer instruments, Atmos. Meas. Tech., 12, 5593–5612, https://doi.org/10.5194/amt-12-5593-2019, 2019.

Huber, D. E., Steiner, A. L., and Kort, E. A.: Daily cropland soil NO_x emissions identified by TROPOMI and SMAP, Geophysical Research Letters, 47, https://doi.org/10.1029/2020gl089949, 2020.

Jang, Y., Lee, Y., Kim, J., Kim, Y. H., and Woo, J.: Improvement China point source for improving bottom-up emission
610 inventory, Asia-Pacific Journal of Atmospheric Sciences, 56, 107–118, https://doi.org/10.1007/s13143-019-00115-y, 2019.

Jo, D. S., Emmons, L. K., Callaghan, P., Tilmes, S., Woo, J., Kim, Y. H., Kim, J., Granier, C., Antonin Soulié, Doumbia, T., Darras, S., Buchholz, R. R., Simpson, I. J., Blake, D. R., Wisthaler, A., Schroeder, J., Fried, A., and Kanaya, Y.: Comparison of urban air quality simulations during the KORUS-AQ campaign with regionally refined versus global uniform grids in the MUlti-Scale Infrastructure for Chemistry and Aerosols (MUSICA) Version 0, Journal of Advances in Modeling Earth
615 Systems, 15, https://doi.org/10.1029/2022ms003458, 2023.

Jordan, C. E., Crawford, J. H., Beyersdorf, A. J., Eck, T. F., Halliday, H. S., Nault, B. A., Chang, L.-S., Park, J., Park, R., Lee, G., Kim, H., Ahn, J.-Y., Cho, S., Shin, H. J., Lee, J. H., Jung, J., Kim, D.-S., Lee, M., Lee, T., Whitehill, A., Szykman, J., Schueneman, M. K., Campuzano-Jost, P., Jimenez, J. L., DiGangi, J. P., Diskin, G. S., Anderson, B. E., Moore, R. H., Ziemba, L. D., Fenn, M. A., Hair, J. W., Kuehn, R. E., Holz, R. E., Chen, G., Travis, K., Shook, M., Peterson, D. A., Lamb,
620 K. D., Schwarz, J. P.: Investigation of factors controlling PM2.5 variability across the South Korean Peninsula during KORUS-AQ. Elementa: Science of the Anthropocene 8(1): 28. DOI: http://dx.doi.org/10.1525/elementa, 2020.

Judd, L. M., Al-Saadi, J. A., Szykman, J. J., Valin, L. C., Janz, S. J., Kowalewski, M. G., Eskes, H. J., Veefkind, J. P., Cede, A., Mueller, M., Gebetsberger, M., Swap, R., Pierce, R. B., Nowlan, C. R., Abad, G. G., Nehrir, A., and Williams, D.: Evaluating Sentinel-5P TROPOMI tropospheric NO_2 column densities with airborne and Pandora spectrometers near New
625 York City and Long Island Sound, Atmospheric Measurement Techniques, 13, 6113–6140, https://doi.org/10.5194/amt-13-6113-2020, 2020.

Judd, L. M., Al-Saadi, J. A., Valin, L., Pierce, R. B., Yang, K., Janz, S. J., Kowalewski, M. G., Szykman, J., Tiefengraber, M., and Müller, M.: The dawn of geostationary air quality monitoring: Case studies from Seoul and Los Angeles, Front. Environ. Sci, 6, https://doi.org/10.3389/fenvs.2018.00085, 2018.

630   Kim, J., Jeong, U., Ahn, M.-H., Kim, J. H., Park, R. J., Lee, H., Song, C. H., Choi, Y.-S., Lee, K.-H., Yoo, J.-M., Jeong, M.-J., Park, S. K., Lee, K.-M., Song, C.-K., Kim, S.-W., Kim, Y. J., Kim, S.-W., Kim, M., Go, S., and Liu, X.: New era of air quality monitoring from space: Geostationary Environment Monitoring Spectrometer (GEMS), Bulletin of the American Meteorological Society, 101, E1–E22, https://doi.org/10.1175/bams-d-18-0013.1, 2020.

Kim, S., Kim, D., Hong, H., Chang, L.-S., Lee, H., Kim, D.-R., Kim, D., Yu, J.-A., Lee, D., Jeong, U., Song, C.-K., Kim, S.-
635   W., Park, S. S., Kim, J., Hanisco, T. F., Park, J., Choi, W., and Lee, K.: First-time comparison between NO_2 vertical columns from Geostationary Environmental Monitoring Spectrometer (GEMS) and Pandora measurements, Atmospheric Measurement Techniques, 16, 3959–3972, https://doi.org/10.5194/amt-16-3959-2023, 2023.

Kim, B.-R., Kim, G., Cho, M., Choi, Y.-S., and Kim, J.: First results of cloud retrieval from the Geostationary Environmental Monitoring Spectrometer, Atmos. Meas. Tech., 17, 453–470, https://doi.org/10.5194/amt-17-453-2024, 2024.

640   Koster, R. D., Darmenov, A. S., and da Silva, A. M.: The Quick Fire Emissions Dataset (QFED): Documentation of Versions 2.1, 2.2 and 2.4, ntrs.nasa.gov, https://ntrs.nasa.gov/citations/20180005253, 2015.

Lambert, J.-C., Keppens, A., Compernolle, S., Eichmann, K.-U., de Graaf, M., Hubert, D., Langerock, B., Ludewig, A., Sha, M.K., Verhoelst, T., Wagner, T., Ahn, C., Argyrouli, A., Balis, D., Chan, K.L., Coldewey-Egbers, M., De Smedt, I., Eskes, H., Fjæraa, A.M., Garane, K., Gleason, J.F., Goutail, F., Granville, J., Hedelt, P., Heue, K.-P., Jaross, G., Kleipool, Q.,
645   Koukouli, M.L., Lorente Delgado, A., Lutz, R., Michailidis, K., Nanda, S., Niemeijer, S., Pazmiño, A., Pinardi, G., Pommereau, J.-P., Richter, A., Rozemeijer, N., Sneep, M., Stein Zweers, D., Theys,, N., Tilstra, G., Torres, O., Valks, P., van Geffen, J., Vigouroux, C., Wang, P., Weber, M.: Quarterly Validation Report of the Copernicus Sentinel-5 Precursor Operational Data Products #18: April 2018 – February 2023, Version 18.01.00, S5P-MPC-IASB-ROCVR-18.01.00-20230403, 196, https://mpc-vdaf.tropomi.eu/ProjectDir/reports//pdf/S5P-MPC-IASB-ROCVR-18.01.00-FINAL.pdf, 2023.

650   Lange, K., Richter, A., Bösch, T., Zilker, B., Latsch, M., Behrens, L. K., Okafor, C. M., Bösch, H., Burrows, J. P., Merlaud, A., Pinardi, G., Fayt, C., Friedrich, M. M., Dimitropoulou, E., Van Roozendael, M., Ziegler, S., Ripperger-Lukosiunaite, S., Kuhn, L., Lauster, B., Wagner, T., Hong, H., Kim, D., Chang, L.-S., Bae, K., Song, C.-K., and Lee, H.: Validation of GEMS tropospheric NO2 columns and their diurnal variation with ground-based DOAS measurements, EGUsphere [preprint], https://doi.org/10.5194/egusphere-2024-617, 2024.

655   Lauritzen, P. H., Nair, R. D., Herrington, A., Callaghan, P., Goldhaber, S., Dennis, J. M., Bacmeister, J. T., Eaton, B., Zarzycki, C. M., Taylor, M. A., Ullrich, P. A., Dubos, T., Gettelman, A., Neale, R., Dobbins, B., Reed, K. A., Hannay, C., Medeiros, B., Benedict, J. J., and Tribbia, J.: NCAR Release of CAM-SE in CESM2.0: A reformulation of the spectral element dynamical core in dry-mass vertical coordinates with comprehensive treatment of condensates and energy, Journal of Advances in Modeling Earth Systems, 10, 1537–1570, https://doi.org/10.1029/2017ms001257, 2018.

660 Lawrence, D. M., Fisher, R. A., Koven, C. D., Oleson, K. W., Swenson, S. C., Bonan, G., Collier, N., Ghimire, B., Kampenhout, L., Kennedy, D., Kluzek, E., Lawrence, P. J., Li, F., Li, H., Lombardozzi, D., Riley, W. J., Sacks, W. J., Shi, M., Vertenstein, M., and Wieder, W. R.: The community land model version 5: Description of new features, benchmarking, and impact of forcing uncertainty, Journal of Advances in Modeling Earth Systems, 11, https://doi.org/10.1029/2018ms001583, 2019.

665 Lee, H., Park, J., and Hong, H.: Geostationary Environment Monitoring Spectrometer (GEMS) algorithm theoretical basis document, NO$_2$ retrieval algorithm, Ministry of Environment. Retrieved from https://nesc.nier.go.kr/en/html/satellite/doc/doc.do, 2020.

Lee, H., Park, J., and Hong, H.: Geostationary Environment Monitoring Spectrometer (GEMS), User's Guide, Nitrogen Dioxide (NO$_2$), National Institute of Environmental Research (NIER), Republic of Korea, December 2022.

670 Levelt, P. F., Joiner, J., Tamminen, J., Veefkind, J. P., Bhartia, P. K., Stein Zweers, D. C., Duncan, B. N., Streets, D. G., Eskes, H., van der A, R., McLinden, C., Fioletov, V., Carn, S., de Laat, J., DeLand, M., Marchenko, S., McPeters, R., Ziemke, J., Fu, D., Liu, X., Pickering, K., Apituley, A., González Abad, G., Arola, A., Boersma, F., Chan Miller, C., Chance, K., de Graaf, M., Hakkarainen, J., Hassinen, S., Ialongo, I., Kleipool, Q., Krotkov, N., Li, C., Lamsal, L., Newman, P., Nowlan, C., Suleiman, R., Tilstra, L. G., Torres, O., Wang, H., and Wargan, K.: The Ozone Monitoring Instrument:
675 overview of 14 years in space, Atmos. Chem. Phys., 18, 5699–5745, https://doi.org/10.5194/acp-18-5699-2018, 2018.

Levelt, P. F., Stein Zweers, D. C., Aben, I., Bauwens, M., Borsdorff, T., De Smedt, I., Eskes, H. J., Lerot, C., Loyola, D. G., Romahn, F., Stavrakou, T., Theys, N., Van Roozendael, M., Veefkind, J. P., and Verhoelst, T.: Air quality impacts of COVID-19 lockdown measures detected from space using high spatial resolution observations of multiple trace gases from Sentinel-5P/TROPOMI, Atmos. Chem. Phys., 22, 10319–10351, https://doi.org/10.5194/acp-22-10319-2022, 2022.

680 Leitch, J., Delker, T., Good, W., Ruppert, L., Murcray, F. J., Chance, K., Liu, X., Nowlan, C. R., Janz, S. J., Krotkov, N. A., Pickering, K. E., Kowalewski, M. G., and Wang, J.: The GeoTASO airborne spectrometer project, Proceedings of SPIE, https://doi.org/10.1117/12.2063763, 2014.

Liu, F., Beirle, S., Zhang, Q., van der A, R. J., Zheng, B., Tong, D., and He, K.: NOx emission trends over Chinese cities estimated from OMI observations during 2005 to 2015, Atmos. Chem. Phys., 17, 9261-9275, 10.5194/acp-17-9261-2017,
685 2017.

Lorente, A., Boersma, F. K., Yu, H., Dörner, S., Hilboll, A., Richter, A., Liu, M., Lamsal, L. N., Barkley, M. P., De Smedt, I., Van Roozendaël, M., Wang, Y., Wagner, T., Beirle, S., Lin, J., Krotkov, N. A., Stammes, P., Wang, P., Eskes, H., and Krol, M.: Structural uncertainty in air mass factor calculation for NO$_2$ and HCHO satellite retrievals, Atmospheric

Measurement Techniques, 10, 759–782, https://doi.org/10.5194/amt-10-759-2017, 2017.

690   National   Institute   of   Environmental   Research   (NIER),   Republic   of   Korea, https://nesc.nier.go.kr/en/html/cntnts/91/static/page.do, last access: 14 February 2024.

Palmer, P. I., Jacob, D. J., Chance, K., Martin, R. V., Spurr, R. J. D., Kurosu, T. P., Bey, I., Yantosca, R., Fiore, A., and Li, Q.: Air mass factor formulation for spectroscopic measurements from satellites: Application to formaldehyde retrievals from the Global Ozone Monitoring Experiment, Journal of Geophysical Research: Atmospheres, 106, 14539-14550,
695   https://doi.org/10.1029/2000JD900772, 2001.

Park, R. J., Oak, Y. J., Emmons, L. K., Kim, C.-H., Pfister, G., Carmichael, G. R., Saide, P. E., Cho, S. Y., Kim, S., Woo, J. H., Crawford, J. H., Gaubert, B., Lee, H., Park, S. Y., Jo, Y. J., Gao, M., Tang, B., Stanier, C. O., Shin, S. S., Park, H. Y., Bae, C., and Kim, E.: Multi-model intercomparisons of air quality simulations for the KORUS-AQ campaign, Elementa, 9, https://doi.org/10.1525/elementa.2021.00139, 2021.

700   Park., J., Lee, H., Hong, H., Van Roozendael, M., Park, R., and Lee, W.-J.: Diurnal Characteristics of the total and tropospheric Nitrogen Dioxide Column over Asia as Observed from GEMS, The 13th GEMS Workshop, Seoul, South Korea, 9–11Nov., 2022a.

Park, J.-U., Park, J.-S., Santana Diaz, D., Gebetsberger, M., Müller, M., Shalaby, L., Tiefengraber, M., Kim, H.-J., Park, S. S., Song, C.-K., and Kim, S.-W.: Spatiotemporal inhomogeneity of total column NO_2 in a polluted urban area inferred from
705   TROPOMI   and   Pandora   intercomparisons,   GIScience   &   Remote   Sensing,   59,   354–373, https://doi.org/10.1080/15481603.2022.2026640, 2022b.

Pfister, G., Eastham, S. D., Arellano, A. F., Aumont, B., Barsanti, K. C., Barth, M. C., Conley, A., Davis, N. D., Emmons, L. K., Fast, J. D., Fiore, A. M., Gaubert, B., Goldhaber, S., Granier, C., Grell, G., Guevara, M., Henze, D. K., Hodžić, A., Liu, X., and Marsh, D. R.: The MUlti-Scale Infrastructure for Chemistry and Aerosols (MUSICA), Bulletin of the American
710   Meteorological Society, 101, E1743–E1760, https://doi.org/10.1175/bams-d-19-0331.1, 2020.

PGN (Pandonia Global Network): Pandonia data archive, http://data.pandonia-global-network.org/, last access: 14 February 2024.

Richter, A., Eyring, V., Burrows, J. P., Bovensmann, H., Lauer, A., Sierk, B., and Crutzen, P. J.: Satellite measurements of NO_2 from international shipping emissions, Geophysical Research Letters, 31, https://doi.org/10.1029/2004gl020822, 2004.

715   Rodgers, C. D.: Inverse Methods For Atmospheric Sounding: Theory and Practice, Series on Atmospheric, Oceanic and

Planetary Physics–Vol. 2., World Scientific, Singapore, 2000.

Schwantes, R. H., Lacey, F. G., Tilmes, S., Emmons, L. K., Lauritzen, P. H., Walters, S., Callaghan, P., Zarzycki, C. M., Barth, M. C., Jo, D. S., Bacmeister, J. T., Neale, R. B., Vitt, F., Kluzek, E., Roozitalab, B., Hall, S. R., Ullmann, K., Warneke, C., Peischl, J., Pollack, I. B., Flocke, F., Wolfe, G. M., Hanisco, T. F., Keutsch, F. N., Kaiser, J., Bui, T. P. V.,
720 Jiménez, J. L., Campuzano-Jost, P., Apel, E. C., Hornbrook, R. S., Hills, A. J., Yuan, Bin, and Wisthaler, A.: Evaluating the impact of chemical complexity and horizontal resolution on tropospheric ozone over the conterminous US with a global variable resolution chemistry model. *Journal of Advances in Modeling Earth Systems*, 14, e2021MS002889. https://doi.org/10.1029/2021MS002889, 2022

Soulié, A., Granier, C., Darras, S., Zilbermann, N., Doumbia, T., Guevara, M., Jalkanen, J.-P., Keita, S., Liousse, C., Crippa, M., Guizzardi, D., Hoesly, R., and Smith, S.: GLOBal ANThropogenic emissions (CAMS-GLOB-ANT) for the Copernicus
725 Atmosphere Monitoring Service simulations of air quality forecasts and reanalyses, Earth System Science Data Discussions, 1–45, https://doi.org/10.5194/essd-2023-306, 2023.

Spinei, E., Whitehill, A., Fried, A., Tiefengraber, M., Knepp, T. N., Herndon, S., Herman, J. R., Müller, M., Abuhassan, N., Cede, A., Richter, D., Walega, J., Crawford, J., Szykman, J., Valin, L., Williams, D. J., Long, R., Swap, R. J., Lee, Y., and
730 Nowak, N.: The first evaluation of formaldehyde column observations by improved Pandora spectrometers during the KORUS-AQ field study, Atmospheric Measurement Techniques, 11, 4943–4961, https://doi.org/10.5194/amt-11-4943-2018, 2018.

Szykman, J. J. and Liu, X.: Tropospheric emissions: Monitoring of pollution (TEMPO) project level 2 science data product validation plan, 2023, https://tempo.si.edu/documents/SAO-DRD-
735 11_TEMPO%20Science%20Validation_Plan_Baseline.pdf

Tang, W., Edwards, D. P., Emmons, L. K., Worden, H. M., Judd, L., Lamsal, L. N., Al-Saadi, J. A., Janz, S. J., Crawford, J. H., Deeter, M. N., Pfister, G., Buchholz, R. R., Gaubert, B., and Nowlan, C. R.: Assessing sub-grid variability within satellite pixels over urban regions using airborne mapping spectrometer measurements, Atmospheric Measurement Techniques, 14, 4639–4655, https://doi.org/10.5194/amt-14-4639-2021, 2021.

740 Tilmes, S., Hodzic, A., Emmons, L. K., Mills, M. J., Gettelman, A., Kinnison, D. E., Park, M., Lamarque, J. -F., Vitt, F., Shrivastava, M., Campuzano-Jost, P., Jiménez, J. L., and Liu, X.: Climate forcing and trends of organic aerosols in the Community Earth System Model (CESM2), Journal of Advances in Modeling Earth Systems, 11, 4323–4351, https://doi.org/10.1029/2019ms001827, 2019.

van Geffen, J., Boersma, K. F., Eskes, H., Sneep, M., ter Linden, M., Zara, M., and Veefkind, J. P.: S5P TROPOMI NO$_2$

slant column retrieval: Method, stability, uncertainties and comparisons with OMI, Atmospheric Measurement Techniques, 13, 1315–1335, https://doi.org/10.5194/amt-13-1315-2020, 2020.

van Geffen, J., Eskes, H., Boersma, K., and Veefkind, J.: TROPOMI ATBD of the total and tropospheric NO_2 data products, Doc.#:5P-KNMI-L2-0005-RP, available at https://sentinel.esa.int/documents/247904/2476257/sentinel-5p-tropomi-atbd-no2-data-products, last access May 15 2024, 2022.

Veefkind, J. P., Aben, I., McMullan, K., Förster, H., de Vries, J., Otter, G., Claas, J., Eskes, H. J., de Haan, J. F., Kleipool, Q., van Weele, M., Hasekamp, O., Hoogeveen, R., Landgraf, J., Snel, R., Tol, P., Ingmann, P., Voors, R., Kruizinga, B., and Vink, R.: TROPOMI on the ESA Sentinel-5 Precursor: A GMES mission for global observations of the atmospheric composition for climate, air quality and ozone layer applications, Remote Sensing of Environment, 120, 70–83, https://doi.org/10.1016/j.rse.2011.09.027, 2012.

Verhoelst, T., Compernolle, S., Pinardi, G., Lambert, J.-C., Eskes, H., Eichmann, K.-U., Fjæraa, A. M., Granville, J., Niemeijer, S., Cede, A., Tiefengraber, M., Hendrick, F., Pazmino, A., Bais, A. F., Bazureau, A., Boersma, F., Bognar, K., Dehn, A., Donner, S., and Elokhov, A. S.: Ground-based validation of the Copernicus Sentinel-5P TROPOMI NO_2 measurements with the NDACC ZSL-DOAS, MAX-DOAS and Pandonia global networks, Atmospheric Measurement Techniques, 14, 481–510, https://doi.org/10.5194/amt-14-481-2021, 2021.

Wiedinmyer, C., Akagi, S. K., Yokelson, R. J., Emmons, L. K., Al-Saadi, J. A., Orlando, J. J., & Soja, A. J. (2011). The Fire INventory from NCAR (FINN): A high resolution global model to estimate the emissions from open burning. Geoscientific Model Development, 4(3), 625–641. https://doi.org/10.5194/gmd-4-625-2011, 2011.

Yang, L. H., Jacob, D. J., Colombi, N. K., Zhai, S., Bates, K. H., Shah, V., Beaudry, E., Yantosca, R. M., Lin, H., Brewer, J. F., Chong, H., Travis, K. R., Crawford, J. H., Lamsal, L. N., Koo, J.-H., and Kim, J.: Tropospheric NO_2 vertical profiles over South Korea and their relation to oxidant chemistry: Implications for geostationary satellite retrievals and the observation of NO_2 diurnal variation from space, Atmospheric Chemistry and Physics, 23, 2465–2481, https://doi.org/10.5194/acp-23-2465-2023, 2023a.

Yang, L. H., Jacob, D. J., Dang, R., Oak, Y. J., Lin, H., Kim, J., Zhai, S., Colombi, N. K., Pendergrass, D. C., Beaudry, E., Shah, V., Feng, X., Yantosca, R. M., Chong, H., Park, J., Lee, H., Lee, W.-J., Kim, S., Kim, E., Travis, K. R., Crawford, J. H., and Liao, H.: Interpreting GEMS geostationary satellite observations of the diurnal variation of nitrogen dioxide (NO_2) over East Asia, EGUsphere [preprint], https://doi.org/10.5194/egusphere-2023-2979, 2023b.

Zara, M., Boersma, K. F., De Smedt, I., Richter, A., Peters, E., van Geffen, J. H. G. M., Beirle, S., Wagner, T., Van Roozendael, M., Marchenko, S., Lamsal, L. N., and Eskes, H. J.: Improved slant column density retrieval of nitrogen dioxide

and formaldehyde for OMI and GOME-2A from QA4ECV: Intercomparison, uncertainty characterisation, and trends, Atmospheric Measurement Techniques, 11, 4033–4058, https://doi.org/10.5194/amt-11-4033-2018, 2018.

Zhang, Y., Lin, J., Kim, J., Lee, H., Park, J., Hong, H., Van Roozendael, M., Hendrick, F., Wang, T., Wang, P., He, Q., Qin, K., Choi, Y., Kanaya, Y., Xu, J., Xie, P., Tian, X., Zhang, S., Wang, S., Cheng, S., Cheng, X., Ma, J., Wagner, T., Spurr, R., Chen, L., Kong, H., and Liu, M.: A research product for tropospheric NO_2 columns from Geostationary Environment Monitoring Spectrometer based on Peking University OMI NO_2 algorithm, Atmos. Meas. Tech., 16, 4643–4665, https://doi.org/10.5194/amt-16-4643-2023, 2023.

Zoogman, P., Liu, X., Suleiman, R. M., Pennington, W. F., Flittner, D. E., Al-Saadi, J. A., Hilton, B. B., Nicks, D. K., Newchurch, M. J., Carr, J. L., Janz, S. J., Andraschko, M. R., Arola, A., Baker, B. D., Canova, B. P., Chan Miller, C., Cohen, R. C., Davis, J. E., Dussault, M. E., and Edwards, D. P.: Tropospheric emissions: Monitoring of pollution (TEMPO), Journal of Quantitative Spectroscopy and Radiative Transfer, 186, 17–39, https://doi.org/10.1016/j.jqsrt.2016.05.008